MIT Joint Program on the Science and Policy of Global Change

Linking Local Air Pollution to Global Chemistry and Climate

Monika Mayer, Chien Wang, Mort Webster and Ronald G. Prinn

Report No. 63
June 2000

The MIT Joint Program on the Science and Policy of Global Change is an organization for research, independent policy analysis, and public education in global environmental change. It seeks to provide leadership in understanding scientific, economic, and ecological aspects of this difficult issue, and combining them into policy assessments that serve the needs of ongoing national and international discussions. To this end, the Program brings together an interdisciplinary group from two established research centers at MIT: the Center for Global Change Science (CGCS) and the Center for Energy and Environmental Policy Research (CEEPR). These two centers bridge many key areas of the needed intellectual work, and additional essential areas are covered by other MIT departments, by collaboration with the Ecosystems Center of the Marine Biology Laboratory (MBL) at Woods Hole, and by short- and long-term visitors to the Program. The Program involves sponsorship and active participation by industry, government, and non-profit organizations.

To inform processes of policy development and implementation, climate change research needs to focus on improving the prediction of those variables that are most relevant to economic, social, and environmental effects. In turn, the greenhouse gas and atmospheric aerosol assumptions underlying climate analysis need to be related to the economic, technological, and political forces that drive emissions, and to the results of international agreements and mitigation. Further, assessments of possible societal and ecosystem impacts, and analysis of mitigation strategies, need to be based on realistic evaluation of the uncertainties of climate science.

This report is one of a series intended to communicate research results and improve public understanding of climate issues, thereby contributing to informed debate about the climate issue, the uncertainties, and the economic and social implications of policy alternatives. Titles in the Report Series to date are listed on the inside back cover.

Henry D. Jacoby and Ronald G. Prinn,
Program Co-Directors

For more information, contact the Program office:

MIT Joint Program on the Science and Policy of Global Change
Postal Address: 77 Massachusetts Avenue
MIT E40-271
Cambridge, MA 02139-4307 (USA)
Location: One Amherst Street, Cambridge
Building E40, Room 271
Massachusetts Institute of Technology
Access: Telephone: (617) 253-7492
Fax: (617) 253-9845
E-mail: *globalchange@mit.edu*
Web site: *http://web.mit.edu/globalchange/*

Printed on recycled paper

Linking Local Air Pollution to Global Chemistry and Climate

Monika Mayer, Chien Wang, Mort Webster and Ronald G. Prinn

Abstract

We have incorporated a reduced-form urban air chemistry model in MIT's 2D-LO coupled chemistry-climate model. The computationally efficient reduced-form urban model is derived from the California Institute of Technology–Carnegie Institute of Technology (at Carnegie Mellon University) Urban Airshed Model by employing the probabilistic collocation method. To study the impact of urban air pollution on global chemistry and climate we carried out three simulations each including or excluding the reduced-form urban model for the time period from 1977 to 2100. In all three runs we use identical emissions, however in the two runs involving the reduced-form urban model the emissions assigned to urban areas are allocated in different ways depending on the scenario we assume for the future development of polluted urban areas. These two simulations are compared to the reference, which does not utilize the reduced-form urban model. We find that the incorporation of the urban air chemistry processes leads to lower global tropospheric NO_x, ozone, and OH concentrations, but to a higher methane mole fraction than in the reference. The tropospheric mole fraction of CO is altered either up or down depending on the projections of urban emissions. The global mean surface temperature is effected very little by the implementation of the reduced-form urban model because predicted increases in CH_4 are offset in part by decreases in O_3 leading to only small changes in overall radiative forcing.

Contents

The authors are associated with the Massachusetts Institute of Technology, Joint Program on the Science and Policy of Global Change, 77 Massachusetts Avenue, Bldg. E40-271, Cambridge, MA 02139-4307, USA.

1. INTRODUCTION

Urban air pollution is not only a regional issue; it is also a global atmospheric chemistry issue. Urban air pollution can alter concentrations of greenhouse gases such as tropospheric ozone directly (*e.g.*, Wang *et al.*, 1986; Hauglustaine and Granier, 1995) or indirectly via changes in the OH free radical concentration (Levy, 1972) and NO_x concentration (Lin *et al*., 1988; Chameides *et al*., 1992; Brasseur *et al*., 1996; Pickering *et al*., 1996). In order to study the impact of urban air pollution on global atmospheric chemistry and climate, a global model interactively coupling submodels of climate, atmospheric chemistry, and economic development can in principle be used. However, atmospheric chemical processes over urban areas are highly nonlinear and differ from those over rural areas in many respects. In addition, lifetimes of many trace species involved, especially NO_x and non-methane volatile organic compounds (NMVOC), are very short ($\leq$ 1 day), and sources of emissions vary on short space scales, so that a spatial resolution $\leq$ 5 km is required for simulations of urban chemical processes in global models. The spatial resolution of most global-scale atmospheric chemistry models currently available is typically > 200 km (in which case urban chemistry is indeed a subgrid-scale process), and their chemical simulations closer to rural than urban chemical processes because of the averaging nature of chemical properties over the model grid volume. In order to model O_3 and OH on a global scale appropriately, a global 3D model should have the following characteristics: 1) resolution < 100 km (1 degree) because of the short life time of NO_x (few days); 2) prognostic rather than diagnostic O_3-HO_x-NO_x-CO-CH_4 background chemistry, especially for CH_4, and the simulation should be transient and longer than 10 years (longer than the lifetime of CH_4); 3) NMVOC chemistry; and 4) reasonable high-resolution multi-year global emission inventories for all necessary anthropogenic and biogenic sources. Unfortunately computational constraints and lack of global high-resolution emission inventories currently limit our ability to model O_3 and OH over time periods in the order of decades. There are several ways to address the problem, and each has its own weaknesses and strengths.

This paper presents a new approach for including urban chemical subgrid-scale processes in a global interactive chemistry-climate model (specifically that of Wang *et al.*, 1998; Prinn *et al*., 1999), by adding a computationally efficient "reduced-form" model for urban air chemistry including NMVOC. The "reduced-form" model consists of a set of analytical expressions derived from the parent urban airshed model aimed to approximate the predictions of the parent model. This significant improvement to the previous model allows us to study the impact of local air pollution on global climate and air chemistry, especially on changes in the global concentrations of tropospheric O_3, NO_x, CO, CH_4, and OH, and to improve the model's predictions regarding tropospheric chemical composition.

This paper first describes the derivation of the reduced-form model for urban air chemistry and its implementation. The impact on global chemistry and climate of extending the chemistry model with the reduced-form model are then discussed, followed by some conclusions regarding the success of the approach.

2. BRIEF DESCRIPTION OF THE MODEL

MIT Integrated Global System Model (Prinn *et al*., 1999) includes an economic development model (the Emission Predictions and Policy Analysis (EPPA) Model) (Yang *et al*., 1996), a two-dimensional land and ocean resolving (2D-LO) interactive chemistry-climate model (Wang *et al*., 1998; Sokolov and Stone, 1998), a terrestrial ecosystems model (Xiao *et al*., 1997), and a natural emissions model. The EPPA model divides the world into 12 regions: the United States, Japan, European Community, other OECD, central and eastern Europe, former Soviet Union, energy-exporting countries, China, India, dynamic Asian economies, Brazil, and rest of the world. The EPPA model is a recursive-dynamic computable general equilibrium (CGE) model that calculates in five-year time steps the anthropogenic emissions of CO_2, CH_4, N_2O, CFCs, NO_x, CO and SO_x as well as a variety of economic variables. When driven with these anthropogenic emissions, and calculated or estimated natural emissions, the 2D-LO atmospheric chemistry-climate model predicts various climate variables as well as the zonally averaged concentrations of major chemically and radiatively important trace species in the atmosphere as a function of time, latitude, and altitude (Wang *et al*., 1998). The chemistry and climate submodels are fully interactive. Specifically, the transport of 18 chemical species ($CFCl_3$, CF_2Cl_2, N_2O, O_3, CO, CO_2, NO, NO_2, N_2O_5, HNO_3, CH_4, HCHO, SO_2, H_2SO_4, hydrofluorcarbons (HFCs), perfluorcarbons (PFCs), sulfur hexafluoride (SF_6), and water vapor) is driven by dynamical variables predicted by the climate submodel. The calculations of 54 gaseous- and aqueous-phase reactions are based on temperatures, radiative fluxes, and precipitation rates computed by the climate model. The gas phase chemistry of the coupled chemistry-climate model consists of three parts: tropospheric O_3-HO_x-NO_x-CO-CH_4 reactions (following Crutzen and Zimmermann, 1991); tropospheric SO_2 sulfate reactions; and stratospheric chlorofluorcarbon and N_2O removal reactions (Wang *et al*., 1998). The current version of the global coupled chemistry-climate model does not include anthropogenic or biogenic NMVOC chemistry. All 54 gaseous- and aqueous-phase reactions included in the global model are listed in the Appendix. We use annually averaged emissions in the global model. For 1990 the annual global (anthropogenic plus natural) emissions are 7 (PgC) as CO_2, 0.6 Pg CH_4, 13 (TgN) as N_2O, no HFCs, 19.9 Gg PFCs, 9.6 Gg SF_6, 0.25 Tg $CFCl_3$, 0.4 Tg CF_2Cl_2, 0.72 (PgC) as CO, 48 (TgN) as NO_x, and 84 (TgS) as SO_2, respectively. In 2100 we use the following global emission rates, 21 (PgC) as CO_2, 1.1 Pg CH_4, 19 (TgN) as N_2O, 1.7 Tg HFCs, 20.5 Gg PFCs, 9.6 Gg SF_6, 21 (PgC) as CO, 92 (TgN) as NO_x, and 125 (TgS) as SO_2, respectively. $CFCl_3$ and CF_2Cl_2 emissions are zero after 2000. A detailed description is given by Wang *et al*. (1998), except for HFCs, PFCs, and SF_6 which are documented in Reilly *et al*. (1999).

Compared to ozone sounding data, the global coupled chemistry-climate model reproduces the general climatology of the latitudinal distribution of ozone outside polluted regions, though it underestimates ozone mole fractions in northern midlatitudes (Wang *et al*., 1998). The OH distributions predicted by the global model provided reasonable simulations of OH-sensitive species like CH_4 or CO, which were compared with ALE/GAGE/AGAGE network measurements. The global averaged OH concentration in the troposphere predicted by the model

(10.4×10^5 radicals/cm^3) is close to the estimate by Prinn *et al*. (1995) based on CH_3CCl_3 measurements (($9.7 - 0.6) \times 10^5$ radicals/cm^3). For more details see Wang *et al*. (1998).

Predicted mole fractions of CO_2, CH_4, N_2O, two CFCs ($CFCl_3$ and CF_2Cl_2), tropospheric O_3, HFCs, PFCs, SF_6, and sulfate aerosols are used to calculate radiative forcing in the climate submodel. Outputs from the chemistry-climate model such as CO_2 concentration, precipitation, surface temperature, and cloud coverage are then utilized by the ecosystem model to calculate important biogeochemical fluxes including net primary and ecosystem production (Xiao *et al*., 1998).

3. THE REDUCED-FORM MODEL FOR URBAN ATMOSPHERIC CHEMISTRY

The 2D-LO global atmospheric chemistry and climate model in its original version (Wang *et al*., 1998) cannot be used to explicitly investigate the interaction between local air pollution and global atmospheric chemistry because: 1) the resolution of the model is much too coarse to resolve urban areas, and 2) it does not include NMVOC chemistry, which is essential for modeling photochemical smog.

The research reported here attempts to solve this problem by creating and implementing in the 2D-LO model a computationally efficient reduced-form of an urban airshed model that is adequate for air-quality simulations. Our version of the reduced-form model is a significantly improved version of the earlier model of Calbo *et al*. (1998). Specifically, the new version includes better input data as well as improvements in the numerical approaches.

3.1 Definition and Characterization of Polluted Urban Areas

In order to derive a numerically efficient, yet reasonably realistic, parameterization to insert in global models, we assume all urban areas in our simulation have the same basic set of chemical reactions and the same size (200 km $\times$ 200 km $\times$ 2 km). However, the meteorological conditions and emissions (provided in our case by the climate submodel and the EPPA submodel, respectively) differ significantly for urban areas in each latitudinal band.

Polluted areas can be characterized by high concentrations of NO_x and NMVOC. Assuming that high mole fractions of these pollutants correlate with high emissions of NO_x and NMVOC, we first employ a global emissions inventory to identify urban areas. We specifically used the global emissions inventory EDGAR (Emission Database for Global Atmospheric Research) version 2.0 of 1990 (Olivier *et al*., 1995). This data set contains, besides other inventories, emissions data for anthropogenic NO_x, CO, NMVOC, and SO_x with a spatial resolution of $1^o \times 1^o$.

A grid cell is counted as an urban area if the EDGAR daily NO_x emissions there are higher than 5 kg N/(day km^2) and the ratio of NMVOC to NO_x emissions ranges from 1 to 9 (Sillman *et al*., 1990). **Figure 1** shows the derived global distribution of highly polluted urban areas in 1990 and the 24 latitudinal bands of the 2D-LO model. Besides the geographic distribution of the NO_x emissions, the range of the emissions and its probability density function (PDF) can be obtained. All emission rates attributed to urban NO_x emitting grid cells were plotted in the form of a histogram in order to get the PDF of urban NO_x emissions. The histogram is then fitted with an

analytical function. To derive the PDFs of urban emissions of NMVOC, CO and SO_2, the map of urban areas derived from the NO_x inventory is applied to the individual EDGAR inventories. Histograms of the emission rates assigned to urban NMVOC, CO, and SO_2 grid cells are created and also fitted with analytical functions. In **Figure 2** the PDFs of NO_x, CO, SO_2, and NMVOC together with analytical fits are shown. The CO, NMVOC and SO_2 data are fitted with normal distributions, and the NO_x data with a lognormal distribution. We will use these fits to define the ranges of possible emission rates per unit area when deriving the reduced-from urban model. We also used the Global Emissions Inventory Activity (GEIA) data set for 1985 (Bouscaren, 1990; Carnovale *et al*., 1992; Dignon, 1992; Kato *et al*., 1992; Saeger *et al*., 1989; Sandnes *et al*., 1992; Spiro *et al*., 1992; Wagner *et al*., 1986) to derive emission PDFs. The GEIA data set has the same resolution as the EDGAR data set but does not include inventories for CO and NMVOC emissions. To derive the emission PDFs using the GEIA data set, only the criterion of high NO_x emissions is applied. We believe this approach is reasonable based on results derived from the EDGAR data set: more than 98% of the high-NO_x emissions grid cells have high NMVOC emissions. The most likely exception would be a grid cell dominated by power plants that produce high NO_x but low NMVOC emissions. In Figure 2, the PDFs and the analytical fits of the GEIA data are plotted. For NO_x and SO_2 emissions the EDGAR and the GEIA data have a similar distribution of urban emissions and as an approximation we could use the analytical PDFs derived from the EDGAR data to fit the GEIA data.

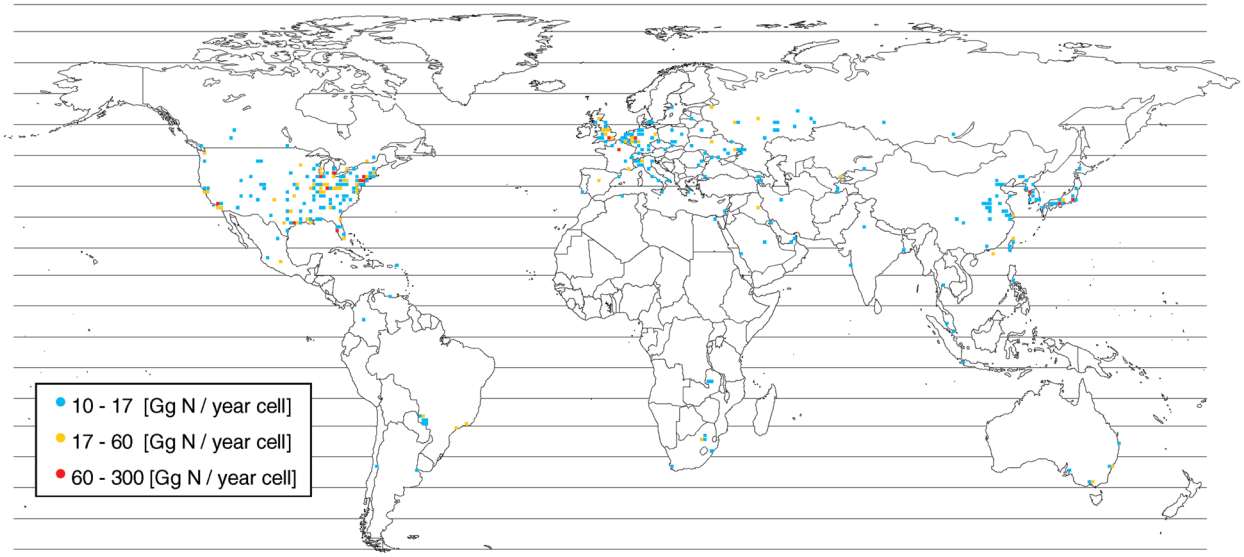

Figure 1. *Global distribution of polluted urban areas represented by NO_x emissions of EDGAR version 2.0 inventory for 1990. The horizontal lines mark the 24 latitudinal bands of the MIT 2D-LO coupled chemistry climate model.*

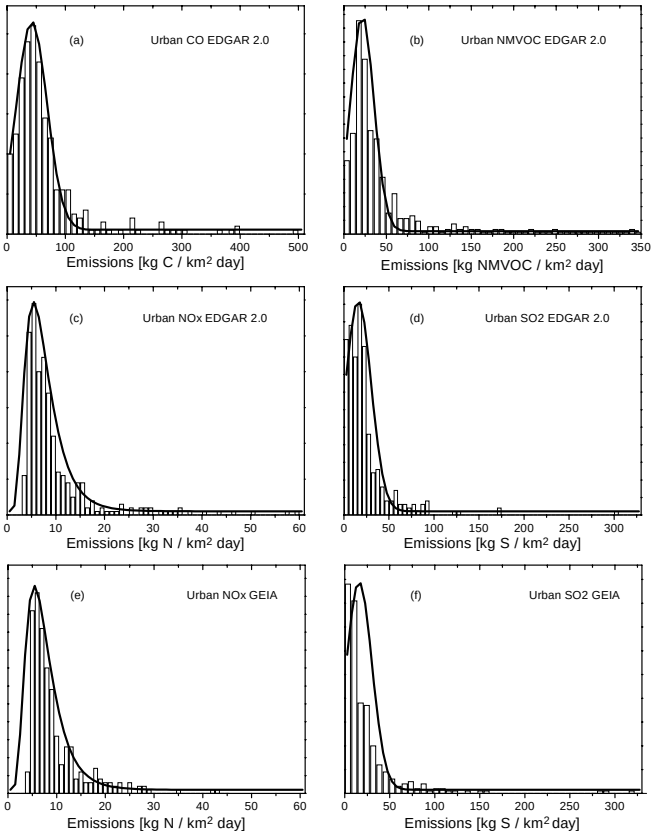

Figure 2. *PDF data and fits for emissions in polluted urban areas of (a) CO, (b) NMVOC, (c) NO_x, and (d) SO_2 derived from the EDGAR inventory, and (e) NO_x and (f) SO_2 derived from the GEIA inventory. CO, NMVOC and SO_2 PDF data are fitted with normal distributions, and NO_x PDF data are fitted with a lognormal distribution. The analytical curves used to fit the GEIA inventory data are the same as for the EDGAR data.*

The quantities of total global emissions attributable to urban areas (hereafter, "urban emissions") for each species at different latitudinal bands can also be calculated. In **Table 1**, the percentage of global emissions from urban areas along with the number of urban areas in each latitudinal band of the 2D-LO coupled atmospheric chemistry-climate model for 1990 are listed. A comparison of the percentages of urban emissions in each latitudinal band derived from the EDGAR and GEIA data set showed the results to be very close, although total emissions for 1990 increased compared to 1985.

Table 1. *The percentage of global emissions attributable to urban areas for NO_x, SO_2, CO, and NMVOCs, and the number of polluted urban areas in several latitude bands, derived from the EDGAR 1990 emissions inventory for the Northern and Southern Hemispheres.*

Latitude	NO_x	SO_2	CO	NMVOC	Urban areas
55°-63° N	38%	36%	32%	21%	18
47°-55°N	51%	43%	37%	45%	69
39°-47°N	52%	41%	40%	44%	93
31°-39°N	49%	46%	34%	40%	99
23°-31°N	30%	24%	13%	13%	34
16°-23°N	21%	26%	9%	13%	9
8°-16°N	5%	8%	3%	4%	3
0°-8°N	6%	4%	2%	4%	3
0°-8°S	2%	3%	2%	3%	1
8°-16°S	14%	3%	13%	10%	2
16°-23°S	14%	6%	13%	13%	7
23°-31°S	32%	33%	14%	24%	6
31°-39°S	47%	54%	31%	43%	8

3.2 Projection of the Evolution of Urban Areas

The procedure we used above to derive the geographical distribution and the PDFs of urban emissions is based on existing emissions inventories and cannot automatically be used for future projections. We adopted a reasonable approach to project the spatial patterns of the urban emissions, based on predictions of total emissions and energy consumption by the EPPA model and urban population projections of the United Nations (UN), with the assumption that the PDFs of pollutant emissions do not change over time. The latter assumption assumes that at sufficiently high levels of emissions, pollution regulations will be established to limit these emissions, as they are currently limited in most of the developed world.

The UN population projections (World Urbanization Prospects, 1998; Long-range World Population Projections, 1992) suggest a worldwide increase in urban population for the upcoming decades. Within the next 10 years, the number of urban dwellers will exceed the number of people living in rural areas. **Figure 3** shows the projections of the urban population for several EPPA regions based on the above UN data for the next century. The percentages of the population living in urban areas in the world and in each EPPA region from 1990 through 2100 are listed in **Table 2**.

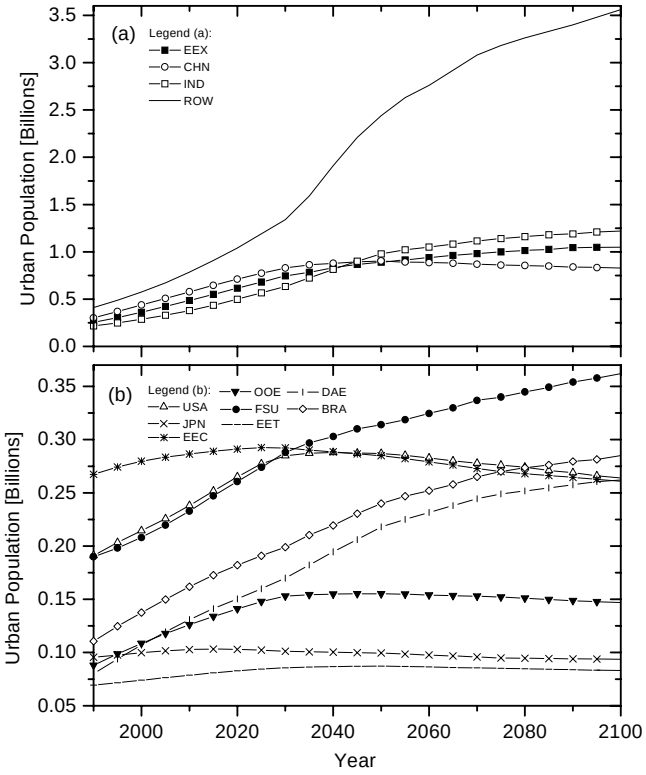

Figure 3*. Urban population projections from 1990 through 2100 for several regions of the economic (EPPA) model; for acronyms of the EPPA regions see Table 2.*

As noted above, urban areas are differentiated from non-urban areas by their high NO_x emissions. To estimate future urban NO_x emissions, we link NO_x emissions to the urban population. We assume that the amount of NO_x emitted from cities is proportional to the product of urban population and energy consumption per capita, which is predicted by the EPPA model. We can then formulate the following equation for urban NO_x emissions ($NO_{x-urban}$) for each EPPA region:

$$NO_{x-urban} = E_C P_{urban} \alpha \qquad (1)$$

where E_C is the regional energy consumption per capita, P_{urban} is the total urban population in the region, and α is a constant of proportionality that does not change over time. The constant α was determined for several EPPA regions for 1990 by deriving $NO_{x-urban}$ from the EDGAR inventory,

E_C from the EPPA model, and P_{urban} from UN statistics. **Table 3** lists the values of α for several EPPA regions. For our calculations of future urban NO_x emissions, an α value of 66 nanogram per Joule has been used, where α is the arithmetic mean of the αs calculated for several EPPA regions. Note that this approach does not permit the inclusion of technology changes, such as catalysts or other energy efficiency advances, which would lead to an emissions reduction per unit of energy consumption.

A different approach was adopted to project urban CO and NMVOC emissions. The two main anthropogenic sources of CO emissions are fossil-fuel combustion and biomass burning in the EDGAR 2.0 inventory for 1990 (Olivier *et al.*, 1995). Economic development in each region changes the relative importance of these two sources. Fossil-fuel combustion increases with development, while biomass burning decreases and can eventually almost disappear in highly developed regions such as the USA (EPA, 1997). This behavior is reflected in the ratio of the percentage of urban NO_x emissions ($NO_{x-\%}$) to the percentage of urban CO ($CO_{\%}$) emissions: a high percentage of urban NO_x and urban CO emissions implies a highly developed economy.

***Table 2**. Projections of the percentage of the population (pop_{urb}) living in urban areas for several EPPA regions through the year 2100 (World Urbanization Prospects, 1998; Long-range World Population Projections, 1992). The greatest increase is projected for non-Annex B countries or regions like, for example, China, India, DAE, and EEX.*

pop_{urb} [%]	**1990**	**2000**	**2020**	**2040**	**2060**	**2080**	**2100**	***Regions***
world	43.2	47.4	56.7	65.6	69.9	72.7	74.5	***EEC***: United Kingdom, Ireland, France, Germany, Netherlands, Belgium, Luxembourg, Spain, Portugal, Italy, Greece, Denmark;
USA	75.2	77.2	82.2	85.5	85.2	85.4	85.2	
JPN	77.4	78.9	83.2	86.2	87.6	88.7	90.3	
EEC	77.8	79.3	83.6	86.6	87.7	88.3	88.4	
OOE	70.2	76.8	83.8	86.4	87.3	87.4	87	***OOE***: Australia, Canada, New Zealand, Turkey, Austria, Sweden, Finland, Norway;
EET	58.5	62.6	71.0	77.6	81.2	83.3	83.9	***EET***: Bulgaria, Czechoslovakia, Hungary, Poland, Romania, Yugoslavia;
FSU	68.5	76.5	75.8	82.8	84.0	86.8	88.9	***FSU***: Former Soviet Union;
EEX	48.6	55.8	67.1	74.3	76.0	77.0	77.8	***EEX***: Iran, Iraq, Kuwait, Saudi Arabia, Venezuela, Qatar, Indonesia, Libya, United Arab Emirates, Algeria, Nigeria, Ecuador, Gabon, Mexico;
CHN	26.2	34.3	49.1	57.9	59.4	59.3	58.9	
IND	25.2	28.4	39.2	53.1	59.8	63.2	65.2	
DAE	47.7	55.7	65.3	72.8	77.2	78.9	79.9	***DAE***: Hong Kong, Philippines, Singapore, South Korea, Taiwan, Thailand; ***ROW***: Rest of the world
BRA	74.7	81.3	87.3	89.6	91.3	92.1	92.6	
ROW	43.2	47.4	56.7	65.6	69.9	72.7	74.5	

***Table 3**. Urban NO_x emissions [teragram N/year], urban population [thousands], and energy consumption per capita [gigajoule/person] for several EPPA regions in 1990. The coefficient α is calculated using Equation 1.*

	USA	**EEC**	**Japan**	**FSU**	**India**	**China**	**Brazil**
Urban NO_x, EDGAR [Tg/y]	5.03	2.58	0.576	1.125	0.156	1.1	0.145
Urban pop. UN [thousands]	186835	272463	95040	189895	230269	380803	112643
Energy/capita, EPPA [GJ]	311.9	141.2	137.4	186.1	10.49	33.06	15.34
α [ng/J]	86.2	67	44.1	32	64.7	87.4	83.9

Figure 4 plots the ratio $NO_{x-\%}$ and $CO_{\%}$ against $NO_{x-\%}$. Data are derived from the EDGAR inventory for 1990 at several latitudinal bands in both the Southern and Northern Hemispheres, where more than three urban areas are present. The quadratic fit of $NO_{x-\%}$ ËCO $_{\%}$ to $NO_{x-\%}$ yields the following relationship that is used to calculate future urban CO emissions:

$$CO_{\%}(t) = \frac{NO_{x-\%}(t)}{3.08 - 0.02 \cdot NO_{x-\%}(t) - 2.64 \cdot \left(NO_{x-\%}(t)\right)^2} \tag{2}$$

Here t is time and $NO_{x-\%}(t)$ is calculated using Eq. 1.

Since NMVOC emissions are not predicted by the EPPA model, the following approximation to predict NMVOC emissions (E_{VOC}) based on CO emissions has been developed:

$$E_{VOC} = (1 + DVOC)(0.2E_{CO} + 0.98) \tag{3}$$

Here, E_{CO} represents CO emissions in kg C per km^2 day, which have the PDF shown in Figure 2a and $DVOC$ is the deviation from the PDF of the CO emissions. $DVOC$ itself is assumed to have a normal distribution, with a mean value of 0.47 kg/(km^2 day) and a standard deviation (σ) of 0.23. The percentages of urban SO_x emissions are always the 1990 values.

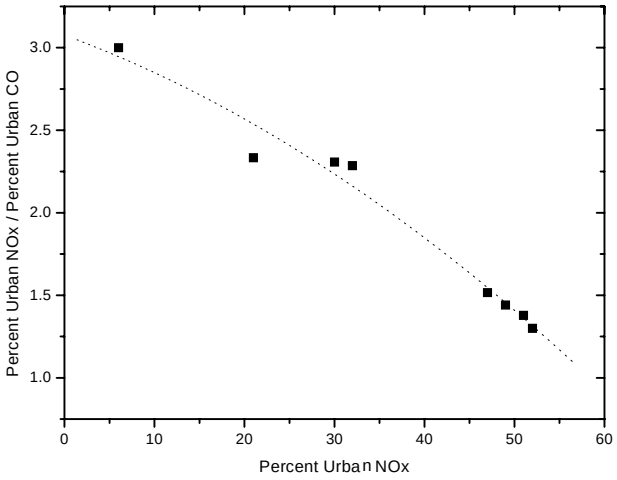

***Figure 4**. Percentage of urban NO_x emissions versus the ratio of urban NO_x to urban CO emissions. The dotted line is a quadratic fit to the data that were derived from the EDGAR 2.0 1990 database.*

As urban populations increase, we expect creation of highly polluted urban areas. To calculate the number of urban areas for years other than 1990, the amount of urban NO_x emissions in each latitudinal band serves as a base. We assume that the PDFs of urban NO_x, SO_x, CO, and NMVOC emissions do not change, and determine an average amount of NO_x emissions E_0 from urban areas in 1990 based on the EDGAR inventory. Given a city of size 200 km $\times$ 200 km, E_0 has a value of 4×10^5 kg N per day. The number of urban areas N in each latitudinal band is then given by the equation:

$$N = \frac{E_{tot}}{E_0} \tag{4}$$

where E_{tot} is the total amount of emissions predicted for the relevant latitudinal band, in kg/day.

3.3 The Urban Airshed Model

The parameterization of urban atmospheric chemistry is based on the California Institute of Technology–Carnegie Institute of Technology (at Carnegie Mellon University) Urban Airshed Model, hereafter referred to as the CIT Model (McRae *et al.*, 1982). The CIT Model solves numerically the atmospheric chemical continuity equation:

$$\frac{\partial C_i}{\partial t} + \nabla \cdot (\vec{u} C_i) = \nabla \cdot (\mathbf{K} \nabla C_i) + R_i + Q_i \tag{5}$$

where C_i is the ensemble mean concentration (mole/volume) of a given species *i*, $\vec{u}$ is wind velocity, $\mathbf{K}$ is the eddy diffusivity matrix, R_i is the chemical production rate of species *i*, and Q_i is the source term for elevated point sources of species *i*. The surface boundary condition is given by the following equation:

$$-\mathrm{K}_{zz} \frac{fC_i}{fz} = E_i - v_g^i C_i \tag{6}$$

The upward flux of each pollutant equals direct emissions subtracted from the dry deposition flux. The vertical eddy diffusivity is K_{zz}, E_i is the ground-level emission flux, and v_g^i is the dry deposition velocity for species *i* (McRae *et al*., 1982).

The chemical formulation used in the CIT Model is a modified version of the condensed Lurmann-Carter-Coyner formulation (Lurmann *et al*., 1987; Harley *et al*., 1993), and includes 35 differential and 9 steady-state chemical species (see Appendix; the isoprene coefficients have not been updated since Carter (1990); for this study we did not include isoprene emissions in our simulations). Nine lumped organic classes represent more than 100 organic species. The 106 reactions in the mechanism include 34 inorganic reactions, all listed in the Appendix. The photolysis reactions of NO_2, NO_3 (two channels), O_3 (two channels), HONO, HCHO (two channels), ALD (acetaldehyde), MEK (methyl ethyl ketone), MGLY (methyl glyoxal), and DIAL (dicarbonyls) are included. The lumping is typically done on a per-mole basis. Some product coefficients are determined by key characteristics of the lumped classes (such as the fraction of terminal alkenes, or the fraction of tri-substituted aromatics). The version of the CIT Model used in this study has been tested against observational data obtained during the 1987 Southern California Air Quality Study (SCAQS) (Harley *et al.*, 1993).

3.4 The Reduced-Form Model for Urban Atmospheric Chemical Processes

To derive the reduced form of the CIT Model, we employed the probabilistic collocation method (Tatang *et al*., 1997) (sometimes also called the deterministic equivalent modeling method). This method approximates a model's response to the uncertain inputs by orthogonal polynomial functions in a chaos expansion. For each output variable, a separate reduced-form model is developed. Compared to traditional statistical methods such as the Monte Carlo Method, the probabilistic collocation method appears to be computationally inexpensive for complex models, which are not highly nonlinear. Calbo *et al*. (1998) showed that the probabilistic collocation method yields reduced forms, which closely approximate the CIT Model.

In this study, urban atmospheric chemistry is parameterized in a 200 km × 200 km urban area with a height of 2.09 km. The model domain has five vertical layers with heights of 73 m, 293 m, 585 m, 1275 m, and 2090 m, respectively. The integration time is 24 hours.

We restrict the total number of input parameters to 15, including: date; latitude; wind speed; temperature; cloudiness; mixing layer height; emissions of NO_x, SO_2, CO, and NMVOC; and

initial and boundary conditions for NO, NO_2, ozone, SO_2, and NMVOC (the latter expressed using an air quality index, AQI as defined by Calbo *et al*., 1998). For several parameters such as temperature, wind speed, mixing layer height, and several chemical emission rates, daily cycles are assumed (Calbo *et al*., 1998). The air temperature is assumed to oscillate –4¡C around the input temperature (daily mean temperature) with a minimum at sunrise and the maximum at 2 PM and linear variations in between. The mixing layer height is equal to the maximum mixing layer height, which is an input value, between 2 PM and sunset. Between 2 hours after sunset and sunrise the mixing layer height is set to be at its nighttime value, 20 times smaller than the maximum or 50 m, whichever is higher. The value of the mixing layer height is linearly interpolated for the time periods between the maximum and minimum value. No spatial variations are assumed for the temperature and mixing layer height fields.

Emission fields of NO_x, CO, and NMVOC (we assume no diurnal variation of SO_2 emissions) have the same daily cycle in addition to their spatial emission patterns. Emissions are assumed to be high during daytime (6 AM – 6 PM) with a maximum at 3 PM and low during nighttime (roughly 4 times lower than daytime values). For more details see Calbo *et al*. (1998). The surface emissions are applied to a circular area with a diameter of 150 km, assuming emissions are highest in the center (8 times the defined input emissions strengths) and decrease gradually toward the perimeter (0.1 times the defined input emissions strengths). We assume further that air entering the modeling domain is clean, and has trace species concentrations typical for remote areas. The fifty-eight model outputs can be summarized in three sets, namely: a) the total aggregated fluxes in a 24-hour period of NO, NO_2, O_3, HCHO, peroxy-acetyl nitrate (PAN), N_2O_5, HONO, HNO_3, CO, SO_2, and SO_3 from the urban modeling domain; b) the moles of NO, NO_2, O_3, HCHO, CO, SO_2, SO_3, and several lumped hydrocarbon species such as ALD2, MEK, ALKA, ETHE, ALKE, TOLU, and AROM (the Appendix defines the acronyms) inside the model domain after a 24-hour simulation; and c) the daily average moles of all 31 species (the first 31 CIT species are listed in the Appendix). The total aggregated net flux over 24 hours is defined as:

$$flux^i_{tot} = flux^i_{out} - flux^i_{in} - depo_i + emiss_i \qquad (7)$$

where $flux^i_{out}$ is the aggregated flux of species *i* out of the domain, $flux^i_{in}$ is the aggregated flux of species *i* into the domain, $depo_i$ is the aggregated dry deposition flux of species *i*, and $emiss_i$ are the aggregated emissions of species *i*. The aggregated fluxes give the effective emissions from urban areas into the global 2D-LO model grid. At the end of the 24-hour simulations the moles of several species are used to initialize the reduced-form models for the next day's runs, and to determine mole fractions at 2D-LO model grid points. Besides moles and fluxes, a variable referring to the maximum ozone mole fraction in the model domain is also computed. This variable (the same as in Calbo *et al*., 1998) is defined as the surface domain-average O_3 mole fraction at the time when the absolute surface peak O_3 occurs. The value of this maximum ozone mole fraction is typically a factor of 2 to 5 higher than the domain-average O_3 mole fraction. The reduced-form urban model is designed to approximate the CIT predictions of 24-hour integrated

fluxes out of the urban modeling domain and total moles in the urban modeling domain at the end of the 24-hour simulation (midnight). Therefore it does not explicitly predict the diurnal variations, though these are fully included in the calculations of the integrated fluxes.

We chose a third-order polynomial chaos expansion including relevant cross terms to obtain the reduced-form model (Calbo *et al*. (1998) did a second-order polynomial chaos expansion). The seasonal dependence of the output variables is expressed as:

$$y_i = y_0^i + \frac{y_0^i}{C_i} \sin\left(\frac{\pi(x - x_c^i)}{w_i} \right) \tag{8}$$

where: y_0^i is the output from the reduced-form model; C_i is a constant determined by fitting CIT Model data and relates to the amplitude of the sine function for output *i*; x is the Julian day; x_c^i gives the phase of the cycle; and w_i is the period (12 months).

The present study uses normal distributions for the PDFs of the emissions (Figure 2) instead of the beta distributions used by Calbo *et al*. (1998) because the global emissions inventory data could be fitted best with normal distributions. We also used the global emissions inventories to derive the PDF of each pollutant separately. This should provide more accurate results and more reasonable coverage of the emissions range than the previous study where only a small data set was employed and a constant proportionality between CO and NMVOC and CO and NO_x emissions was assumed (Calbo *et al*., 1998). As a result, our NO_x emissions are in the range from 0 – 60 kg N/(km^2 day) with a mean of 6 kg N/(km^2 day) whereas Calbo *et al*. (1998) defined a range from 0 – 115 kg N/(km^2 day) with the mean of 23 kg N/(km^2 day). The CO range is the same in both studies (0 – 500 kg C/(km^2 day)) but our mean value of 50 kg C/(km^2 day) is half the value of Calbo *et al*. (1998). The new NMVOC emissions range from 0 – 350 kg NMVOC/(km^2 day) with a mean of 22 kg NMVOC/(km^2 day) in contrast to Calbo *et al*. (1998) who had 0 – 160 kg NMVOC/(km^2 day) with a mean of 33 kg NMVOC/(km^2 day). Finally, our SO_2 emissions are assumed to be between 0 and 330 kg S/(km^2 day), compared to Calbo *et al*. (1998) who used the range of 0 – 50 kg S/(km^2 day), but in both studies the same mean, namely 11 kg S/(km^2 day), is derived.

Another major improvement is a change in the initial profiles of the pollutants compared to Calbo *et al*. (1998), who assumed pollutants at the beginning of each model day existed only in the first two model layers. The new profiles include all five model layers. This is of importance especially for species like ozone or CO because the boundary conditions determine also the incoming flux into the urban domain. This change in the initial profiles most affects ozone production and related processes such as the formation of PAN.

Comparisons between results of the reduced-form model and those of the parent CIT Model are shown for selected outputs in **Figure 5**. The set of input values chosen for the comparison is different from the (collocation) values used to derive the reduced-form model. The selected testing data cover the whole range of the input parameters but the sampling was not done in a way that reflects exactly the PDFs. However more points are chosen in the high probability ranges. All results in Figure 5 are derived for Julian day 181.

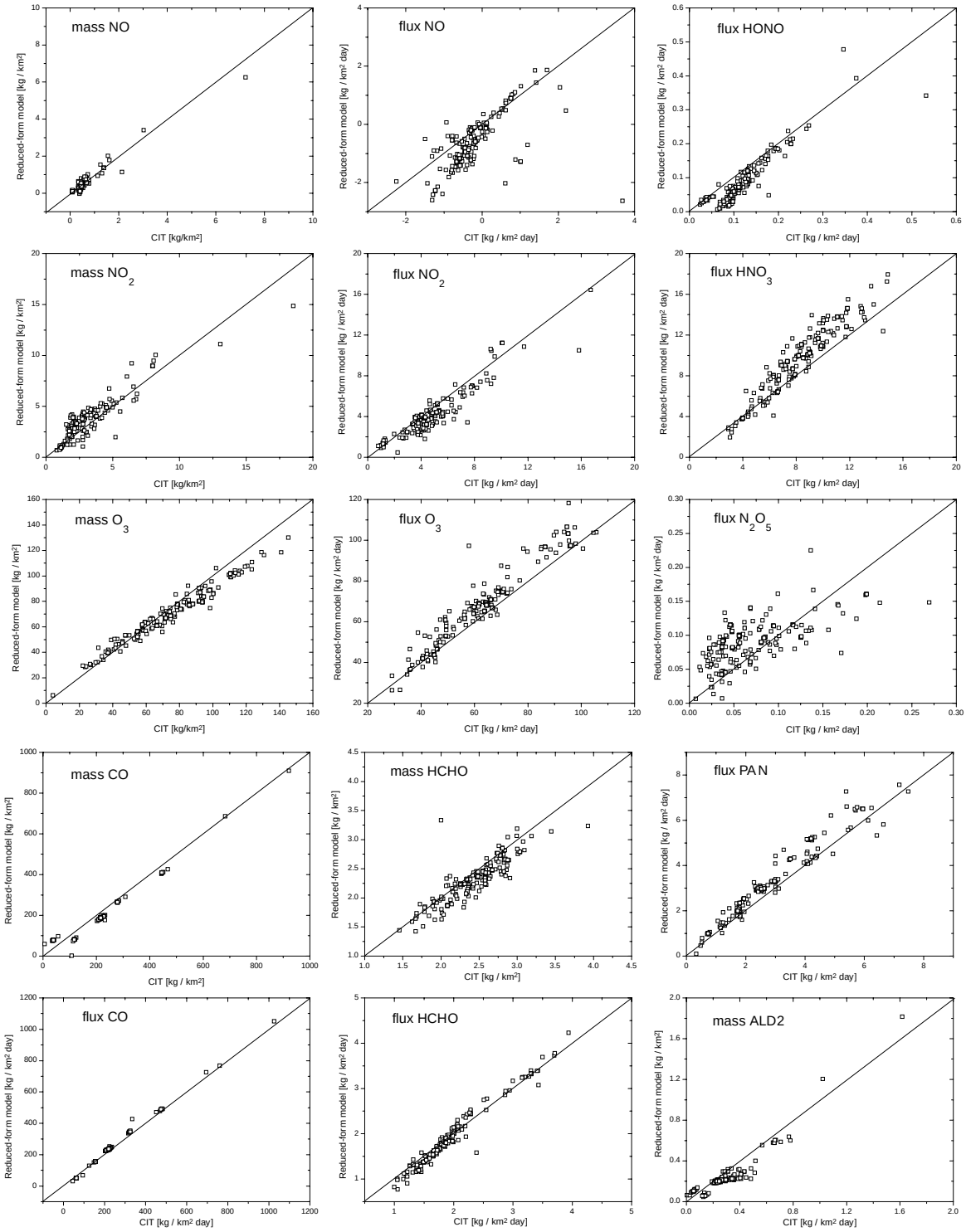

Figure 5*. Comparison between reduced-form urban model results and parent CIT Model results. Input values are different from those used to derive the reduced-form urban model. The fluxes are defined as the total aggregated net fluxes per km^2 over 24-hours out of the urban domain; masses are the total mass per km^2 in the urban domain at the end of the 24-hour simulation. For species acronyms see Appendix, for peak ozone definition see text.*

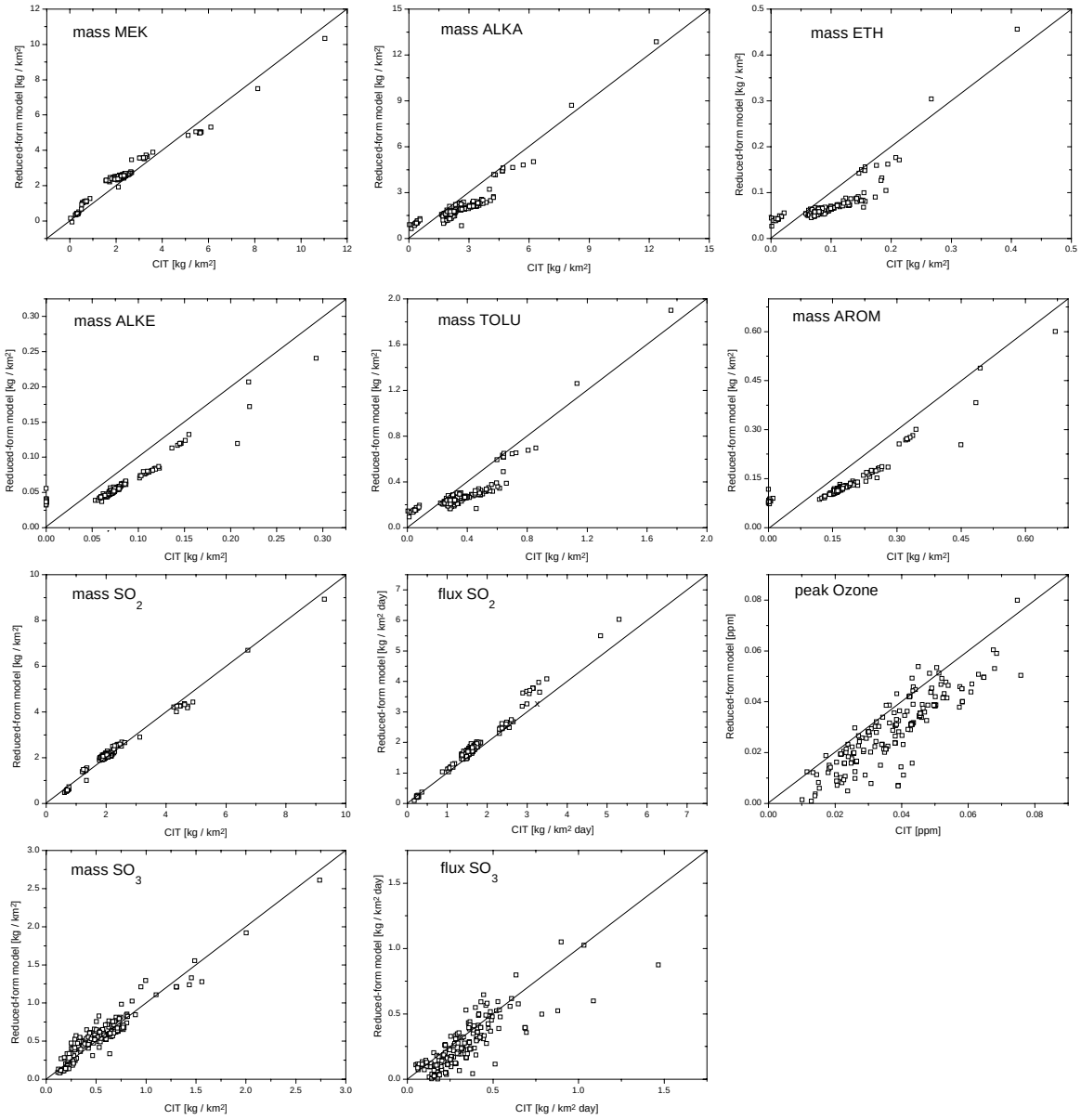

Fig. 5 (continued)*. Comparison between reduced-form urban model results and parent CIT Model results.*

Compared to Calbo *et al*. (1998) we get generally better correlations between the output of the reduced-from model and the CIT Model. For some species the improvement is extremely obvious (*e.g*., the flux of CO or PAN in Figure 5). The results differ in both studies, mainly because of changes of the emissions PDFs but also because of differences in the initial vertical profiles of several pollutants. Our mean values of the emissions PDFs tend to be lower than the Calbo *et al*. (1998) estimates. In the present study the peak ozone concentrations are substantially higher than the values published by Calbo *et al*. (1998). This is because new initial vertical profiles of the pollutant concentrations (especially ozone) were introduced. The results of this study are more realistic than the results of Calbo *et al*. (1998) based upon comparisons to observations.

4. LINKING THE REDUCED-FORM MODEL WITH THE GLOBAL CHEMISTRY-CLIMATE MODEL

The reduced-form urban atmospheric chemistry model is incorporated into the interactive 2D-LO chemistry-climate model as a subroutine. Data is communicated between these two every 24 hours. The global model supplies the reduced-form urban models with meteorological data, including wind speeds, temperatures, mixing layer heights, and cloud coverages. The total anthropogenic emissions calculated by the EPPA model are mapped from the EPPA economic regions to the 24 latitudinal bands through use of a population density map (Fung *et al*., 1991). The anthropogenic emissions originally input directly into the global model are now separated into urban emissions, which are supplied to the reduced-form models, and rural emissions, which go into the global model simulations. **Figure 6** schematically represents the implementation of the modeling scheme.

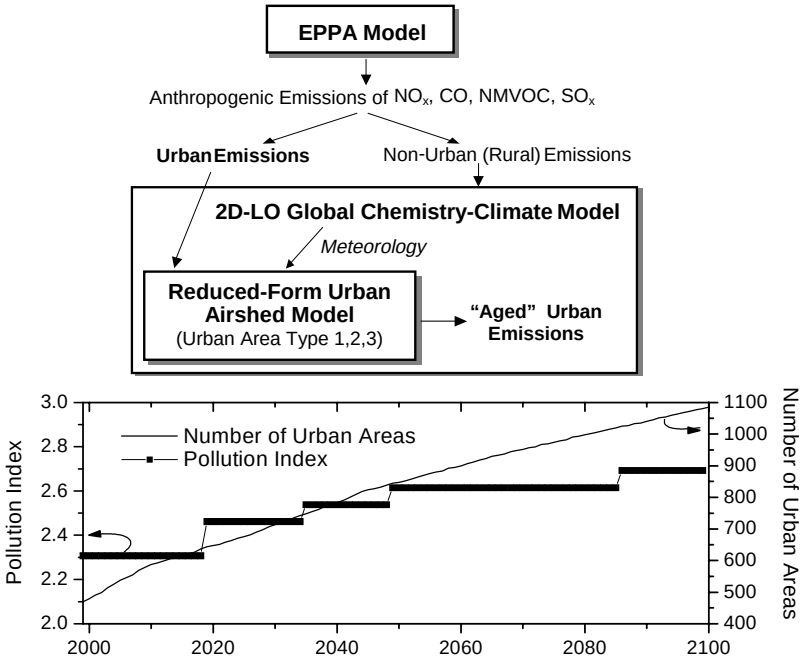

Figure 6*. Schematic showing the implementation of the reduced-form urban model in the global 2D-LO chemistry-climate model. At the bottom the projections of the increase of the number of urban areas and change of the pollution index of theurban areas is shown. For detailed description see text.*

In order to save computational time, while still representing reasonably the different characters of cities with regard to emissions, we have assumed three types of urban areas with low (1), medium (2), and high (3) levels of pollution, respectively. Currently, we assume that the low, medium, and highly polluted cities account for 75%, 20%, and 5%, respectively, of all cities within any latitudinal band. Their emissions can be derived by multiplying the average emissions per urban area, E_0 (Eq. 4), with a weighting coefficient, γ_i. The coefficient γ_i guarantees that the sum of emissions for the three city types equals the total amount of urban emissions. We have defined five γ_i. Three (γ_1 , γ_2 , γ_3) are used for urban area type 1, 2, and 3 when there are 20 or more polluted cities in the latitudinal band. Two (γ_4 and γ_5) are used for latitudinal bands with less than 20 and more than 4 urban areas; only low- and medium-polluted cities are assumed. For the latitudinal bands in which fewer than four urban areas are located, only one type is assumed, and emissions are set equal to E_0. **Table 4** lists the assumed values for γ_i. Over time we expect relatively more medium and highly polluted urban areas. At the bottom of Figure 6 the predicted increase of

urban areas over time is shown in addition to the time development of the global average of a so-called pollution index (PI). The PI reflects the number of types of urban areas found in each latitudinal band. It is one if we have only low polluted urban areas (type 1); two if we have low and medium polluted urban areas (type 1 and 2), and three if we have all three types of urban areas (type 1, 2, and 3). The global average PI is the arithmetic mean of the PIs of the 13 latitudinal bands where we allocate urban areas. It is a step function because we assume three discrete types of urban areas.

Table 4*. Weighting coefficients for the three types of urban areas.*

γ_1	γ_2	γ_3	γ_4	γ_5
0.8	1.25	3	0.8	1.6

For each latitudinal band of the 2D-LO global model, up to three urban reduced-form models are executed to provide fluxes and moles relevant to the types of urban areas. The total contribution of urban areas to emissions to be input into the global model and the chemical tracer concentrations to be input at the next iteration of the reduced-form model is then obtained. First we multiply the fluxes and moles of trace chemicals for each type of urban area by the total number of such areas within the latitudinal band, and second, we sum the aged emissions or average the mole fractions thus obtained for all three types of urban areas.

After both global and urban models have completed their daily integrations at midnight, the fluxes from the urban models are used as emissions to be added to the rural emissions supplied to the global 2D-LO model for its next day's integration. At the same time, the mole fractions of chemical species at the grid points of the global model in its lowest three layers are updated by combining, with mass-weighting, the total moles of the species in both urban and rural areas, as predicted by the two models separately and dividing by the total moles of air in the lowest three layers.

Initial conditions in the urban domains for the next day's simulations are set by air quality indices (AQIs) for NO, NO_2, ozone, SO_2, and NMVOC, derived using the moles of these species in the urban domains at the end of the 24-hour simulations. The AQI is a measure of how many moles of a certain species are present in the modeling domain. If we calculate the AQI at the end of a 24-hour simulation, we have a measure of the moles of that certain species in the modeling domain at the end of our run. Since we assume that the shapes of the initial vertical profiles of several species do not change, we can obtain initial and boundary conditions for a compound for a given AQI. These AQIs have a beta distribution ranging from 0 to 1, where 1 denotes a highly polluted atmosphere. The AQI for a species is 1 when the mole fraction reaches 100 ppb for NO, 300 ppb for NO_2, 100 ppb for SO_2, 250 ppb for O_3, 40 ppb for HCHO, 20 ppb for ALD2, 22 ppb for MEK, 95 ppb for ALKA, 28 ppb for ETHE, 18 ppb for ALKE, 20 ppb for TOLU, and 8 ppb for AROM (Finlayson-Pitts and Pitts, 1986; Seinfeld and Pandis, 1998). For the NMVOC, the AQI is the sum of the AQIs of HCHO, ALD2, MEK, ALKA, ETHE, ALKE, TOLU, and AROM. To calculate the AQIs, the moles of pollutants in the urban domains must be converted to mole fractions. The AQI is defined for each species as:

$$AQI = \frac{m \cdot R \cdot T}{p \cdot \xi_{\max}} \tag{9}$$

where m is the molar concentration of the pollutant in the urban domain, R is the gas constant, T is the temperature, p is the pressure, and $\xi_{\max}$ is the mole fraction of the species when its AQI is unity.

5. EFFECT OF LOCAL AIR POLLUTION ON GLOBAL CHEMISTRY AND CLIMATE

To investigate the impact of urban air pollution on global chemistry and climate, we carried out three different simulations with the coupled 2D-LO chemistry-climate model. All three runs use the same emissions predictions derived from the EPPA model, which assume no policy actions to explicitly reduce or cap future anthropogenic emissions. The total emissions of CO and NO_x provided by the EPPA model are shown in **Figure 7**. (Note that NO_x emissions are expressed in units of Tg N per year, whereas CO emissions are expressed in units of Tg CO per year.) All three simulations begin in 1977 and end in 2100. The period from 1977 to 1990 is devoted to model spin-up.

The first simulation (the reference run) was done with the 2D-LO global coupled chemistry-climate model, without the reduced-form urban chemistry model. The second and third simulations were carried out using the global model in conjunction with the reduced-form urban model. The two latter runs differed in that, in one case (referred to as META), the number of urban areas and partitions of urban emissions were fixed at their 1990 values (see Table 1). Total and urban emissions in META are therefore predicted to grow at the same rate. In the other case (referred to as META-TIME), the number of urban areas (Fig. 6, **Figure 8**) as well as the partitioning between urban and non-urban emissions changes through 2100. Total emissions are the same as in the reference and the META run, but total urban emissions for NO_x, NMVOC, and CO are higher than in the

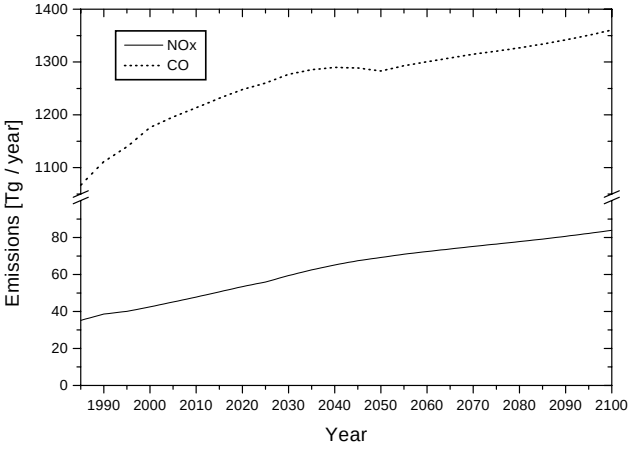

***Figure 7**. Total anthropogenic NO_x and CO emissions predicted by the economic model (EPPA) from 1985 through 2100 assuming no policy actions to reduce or cap anthropogenic emissions.*

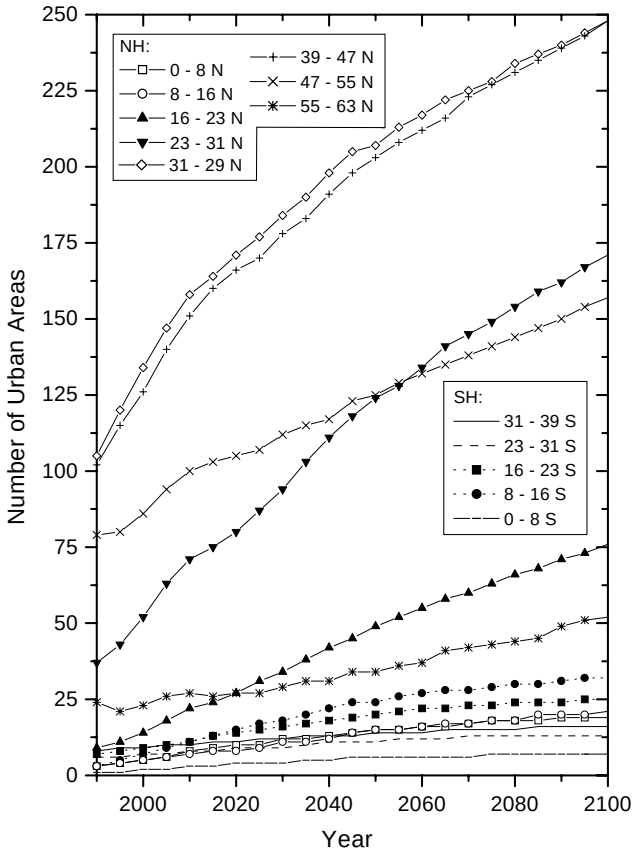

***Figure 8**. Projected number of polluted urban areas for several latitudinal bands from 1990 through 2100. Those projections are used in the META-TIME run.*

META run. The emissions per city of several pollutants increased substantially over time in the META run. In the META-TIME run, however, the projected number of polluted urban areas increases so that emissions per type of urban area over time remain practically constant. The total predicted number of urban areas in 2100 for this run is about three times the number in 1990 (see Fig. 6), although for specific latitudinal bands (*e.g.*, $8^o - 16^oS$ and $16^o - 23^oN$), the number of cities could be eight or even sixteen times higher in 2100 than in 1990 (Fig. 8). Our prediction also shows that in 2100, most urban areas will still be in the Northern Hemisphere midlatitudes. The projected partitioning between urban and rural emissions changes substantially over time (**Figure 9**) primarily because of the increase in urban population (Fig. 3). Note that in this study, NMVOC emissions are related to CO emissions (Eq. 3), so urban NMVOC percentages are not calculated separately from CO.

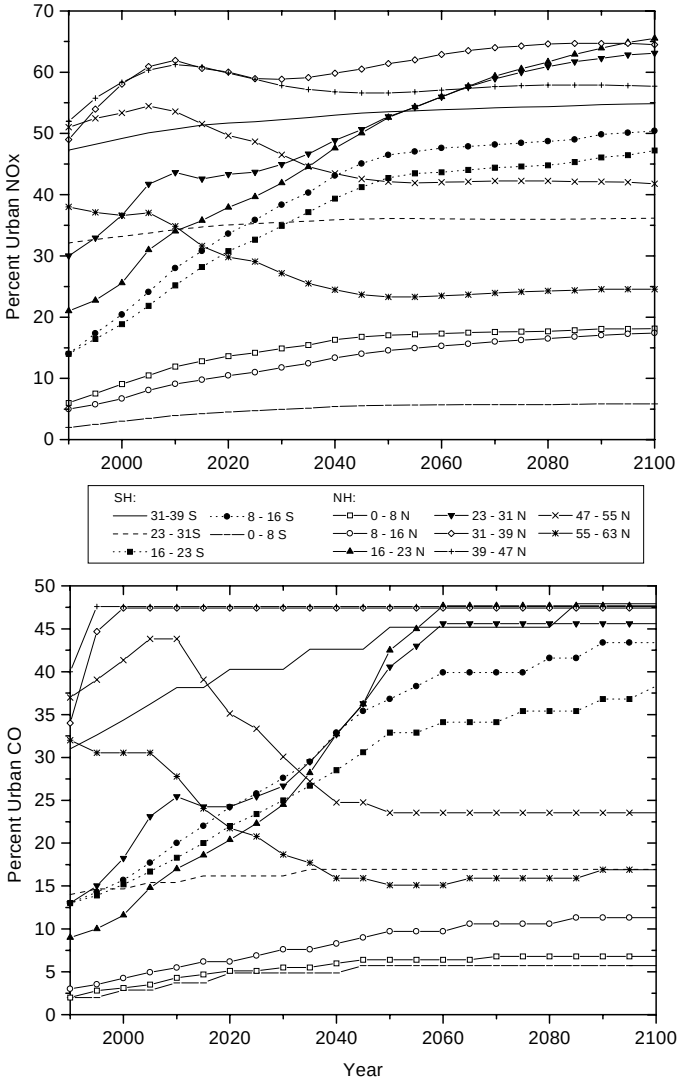

***Figure 9**. Projected percentage of total emissions emitted in urban areas for NO_x and CO for several latitudinal bands from 1990 through 2100. In the META-TIME run these projections are used whereas in the META run the 1990 values 1990 of Table 1 are used throughout 1990 to 2100.*

The effects of including urban processes using the reduced-form model on the global annual average tropospheric NO_x and ozone mole fractions, and the global annual average tropospheric OH concentration for the META and META-TIME runs are shown in **Figure 10**. Levels of all three species are found to be reduced compared to the reference run, and the effect on global concentrations is always more significant in the META-TIME run than in the META run. Note that the reason we can see in Figure 10 an immediate difference between the reference run and the two runs using the urban chemistry model is because we plot annual averages, and the lifetimes of all three species in Figure 10 are much shorter than one year. The regional reductions in tropospheric ozone due to the consideration of the urban chemistry are much greater (up to minus 20% compared to the reference) than on global average (up to minus 10%). In **Figure 11** the change in percent for the

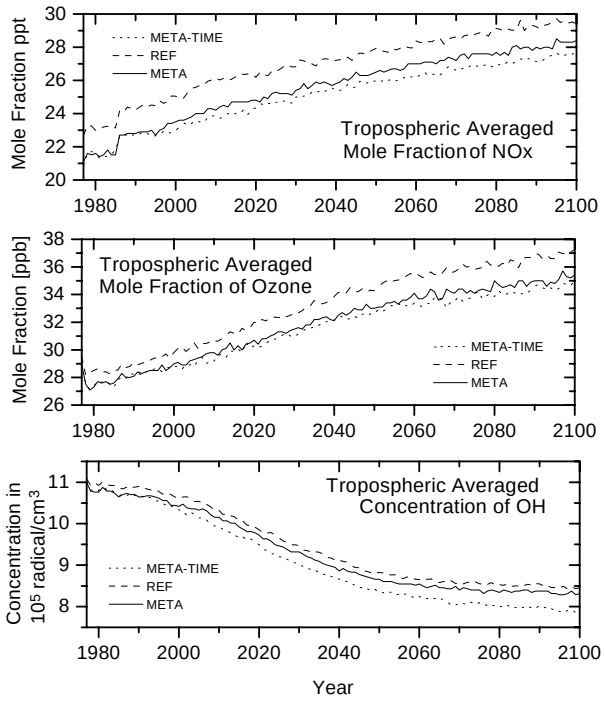

Figure 10. *Global average tropospheric NO_x and O_3 mole fraction, and OH concentration from 1977 to 2100 for the reference run, and the META and META-TIME runs.*

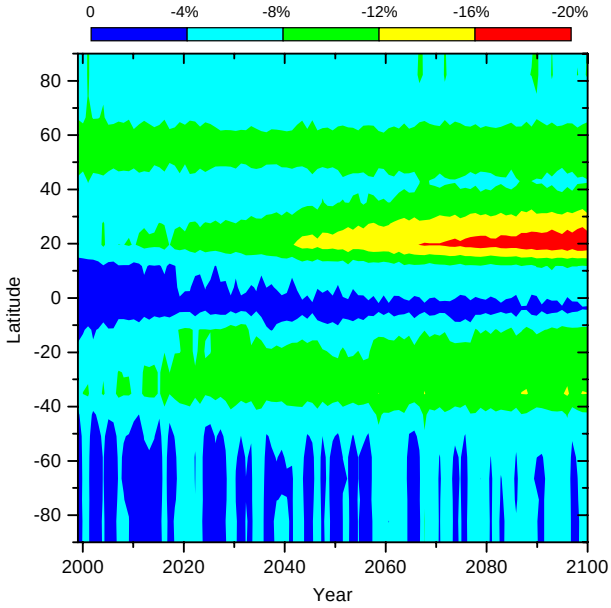

Figure 11. *Change in percent of the global average tropospheric O_3 mole fraction for the META-TIME run compared to the reference. Due to the consideration of urban chemistry processes the global tropospheric ozone mole fraction decreases.*

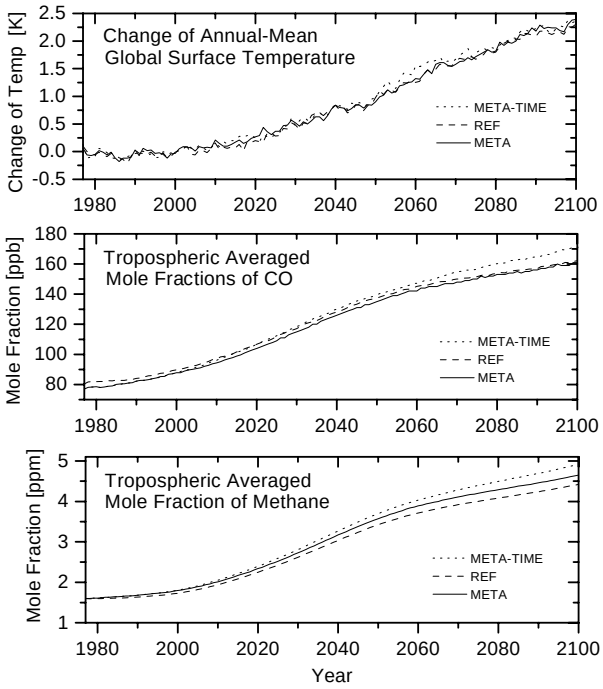

Fig. 12. *Global average tropospheric mole fractions of CO and methane and the global mean surface temperature from 1977 to 2100 for the reference, META, and META-TIME runs. The global mean surface temperature is shown relative to the global mean surface temperature of the reference run in 1990.*

META-TIME run compared to the reference run is plotted for the period from 1999 to 2100. The decrease in ozone is most pronounced at latitudes where large urbanization rates are projected (see also Fig. 9).

From **Figure 12**, we see that the global annual average mole fraction of CH_4 increases faster when urban processes are included due to the greater decrease in the average tropospheric OH concentration in the two urban cases. The global annual average tropospheric CO mole fraction is also shown in Figure 12. Depending on the scenario for urban area development, we see either a slightly smaller CO mole fraction in the META run, or higher CO mole fraction in the META-TIME run after 2030.

The changes in global tropospheric mole fraction of ozone and methane influence

radiative forcing. Our simulations show an increase in CH_4 and a decrease in O_3 in the troposphere, to different extents in the two runs where urban processes are included. For example, in 2100 the tropospheric averaged mole fraction of CH_4 is about 0.5 ppm higher (META-TIME run) or 0.2 ppm higher (META run) than in the reference run. In Figure 12, the change in the annual-mean global surface temperature relative to the annual-mean global surface temperature of 1990 is shown for the period from 1977 through 2100. If we fix the number of urban areas (META run), we are unable to see a clear change in surface temperature compared to the reference run. Altering the number of cities (META-TIME run) gives slightly higher surface temperatures after 2050. In order to understand the differences between the two simulations, META and META-TIME, we have analyzed fluxes and mole fractions in the urban domains for NO_x and NO_y species (in this study, NO_y refers to the sum of PAN, HNO_3, HONO, and N_2O_5), CO, and ozone.

5.1 NO_x and NO_y

We assumed that, among the total urban NO_x emissions, 95% are emitted as NO and 5% as NO_2. **Figure 13** shows the total emissions of NO, NO_2, PAN, and HNO_3 after chemical processing from urban areas (we will call these Òaged Ó emissions) as functions of latitude in 1990, 2050, and 2100 for the META-TIME run. The aged emissions are the aggregated fluxes from the 24-hour simulation (see Eq. 7 and related text) averaged over the three different city types (low, medium, and highly polluted). All fluxes are expressed in units of Gg N per day. In our analysis PAN is the dominant species in the aged emissions in the Northern Hemisphere and NO_2 in the Southern Hemisphere. In 2100 the flux of all aged nitrogen-containing species is about double that in 1990. In addition the latitudinal distribution of the fluxes changes and more weight is found at Northern Hemisphere lower latitudes. The aged emissions shown in the top panel (for 1990) of Figure 13 are also the results for the META run since in that year the assumptions regarding urban emissions are the same as for the META-TIME run. For the META-TIME run, the aged emissions of NO_y increase proportionally to NO_x emissions, whereas in the META run, NO_y fluxes and their latitudinal distributions do not change to that extent.

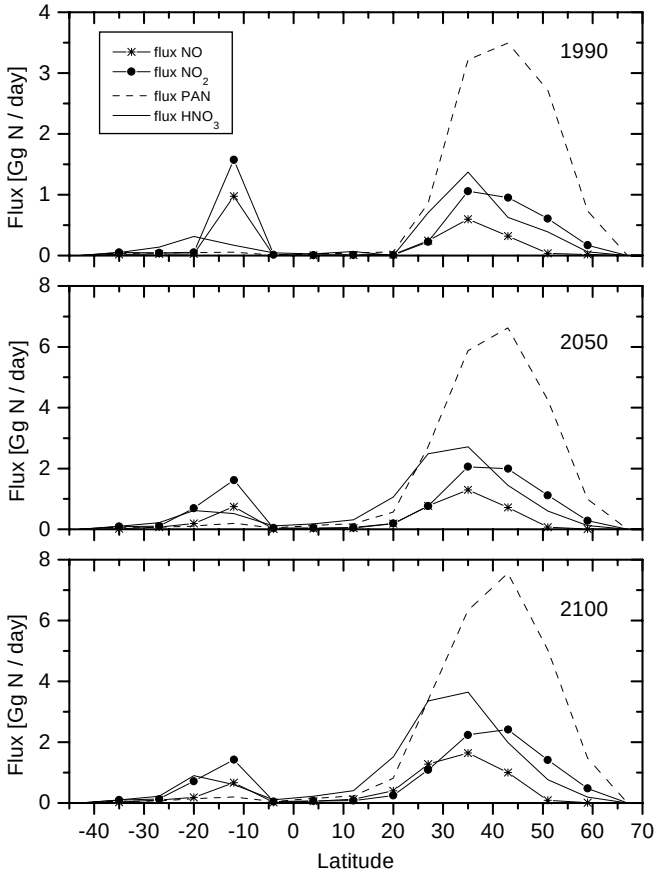

***Figure 13**. Latitudinal distribution of annual average fluxes of NO, NO_2, PAN, and HNO_3 exported from urban domains after chemical processing for the META-TIME run for 1990, 2050, and 2100. Note that in 1990 the vertical axis extend only to 4 Gg N/day whereas in 2050 and 2100 it is 8 Gg N/day.*

The differing behaviors of aged emissions in the META-TIME and META runs are due to the strong nonlinearity of the chemistry. This can be seen more clearly in the temporal behavior of the fluxes from the urban areas and in the mole fractions of NO, NO_2, PAN, HNO_3, HONO, N_2O_5 in the urban domains (**Figure 14**). The mole fractions shown in the bottom panels are the 24-hour and urban domain (200 km $\times$ 200 km $\times$ 2 km) averages of all three types of cities and all latitudinal bands. (Note that actual surface mole fractions are higher than these averages.) Fluxes in the META-TIME run increase with time, mainly due to the increase in the number of cities. Mole fractions, however, fluctuate throughout the simulation and do not show the same significant increase as is apparent for fluxes. The NO mole fraction varies most obviously among all nitrogen-containing species with sudden changes coinciding with the introduction of a new type of city in one or more latitudinal bands. This causes a different allocation of the emissions between low, medium, and highly polluted cities within a latitudinal band leading to different average mole fractions for this latitudinal band. Because we calculate the global average mole fraction as the arithmetic mean of the 13 latitudinal average mole fractions, transitions from a one to a two type urban scenario (*i.e*. from three to four cities) in a single latitudinal band can be seen in the global average (the NO_x emissions in the medium polluted urban areas are about two times higher than in the low polluted case). The more cities we project over time the smaller the fluctuations become because eventually in almost all latitudinal bands the 3 different types of urban areas are represented, which is also reflected in an increase of the pollution index plotted in Figure 6. The observed abrupt changes in the mole fractions coincide in time with the change of the pollution index for the time period after 1990. In real world of course smooth variations will be observed.

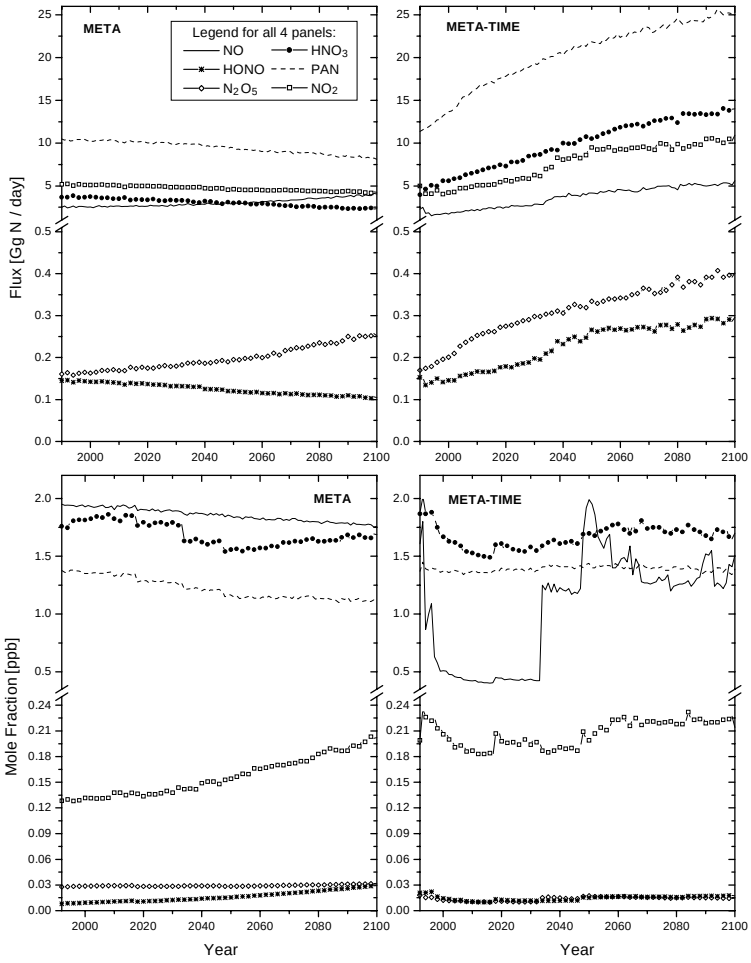

Figure 14*. Global annual average fluxes exported from urban domains and mole fractions in urban domains of NO, NO_2, PAN, HNO_3, HONO, and N_2O_5 for the META and META-TIME runs from 1990 to 2100.*

The behavior of the mole fractions of NO_x and NO_y in the META differs from that of the mole fractions in the META-TIME run discussed above. In the META run the emissions per urban area are increased steadily but no new urban areas are added and the fluctuations of the mole fractions are therefore smaller. The NO_x mole fraction in the META run actually decreases over time although NO_x emissions increase. In 2100, the mole fractions of all NO_y and NO_x species predicted by the META run are higher than those predicted by the META-TIME run with the exception of PAN and NO_2.

5.2 Ozone

In **Figure 15** the latitudinal distribution of the annual mean 1-hour peak ozone mole fractions averaged over all three types of urban areas for the META and META-TIME runs are plotted for the period from 2000 to 2100. For the META-TIME run we find that at latitudinal bands where initially all three types of urban areas are present (*e.g.*, northern midlatitudes), the peak ozone is quite constant over time due to our assumption that the emission rates for each type of urban area do not change over time. In contrast, at latitudinal bands where we introduce medium and/or highly polluted urban areas in the course of the run, the peak ozone increases abruptly (see also changes in the pollution index, Fig. 6). The aggregated ozone fluxes grow as urban areas increase in the META-TIME run (roughly, by a factor of 3), in contrast to the decrease in ozone fluxes found in the META run (Figure 15).

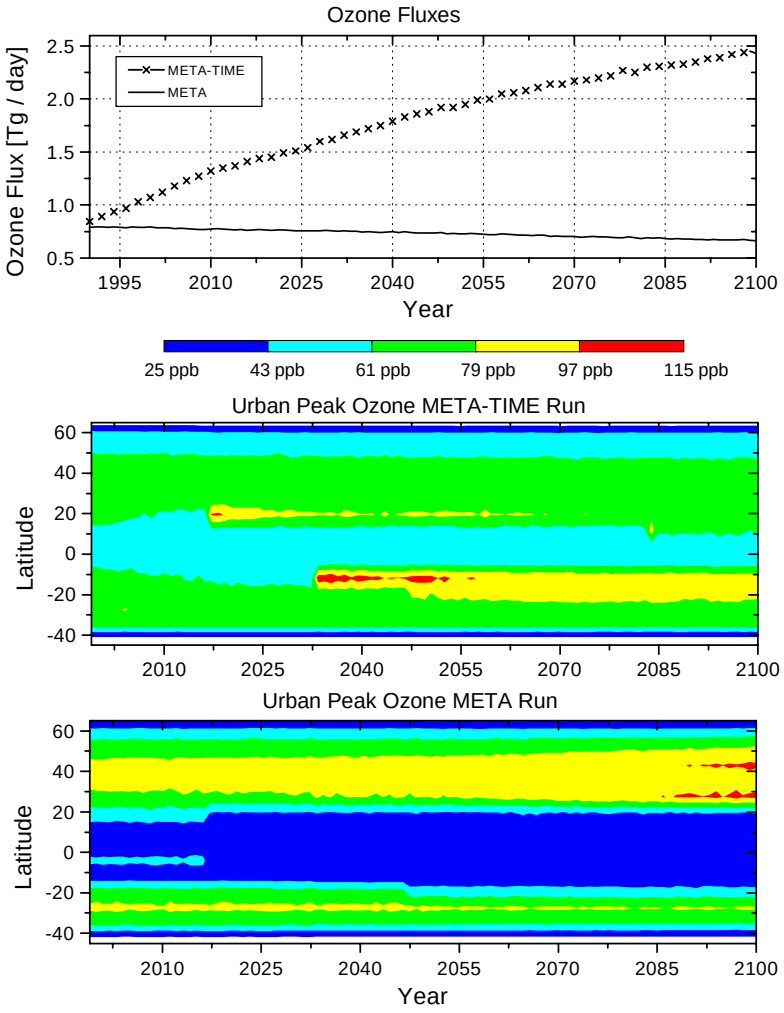

Figure 15*. Global annual average ozone fluxes exported from urban domains from 1990 through 2100 and the latitudinal distribution of the annual average peak ozone mole fractions in urban domains for the META and META-TIME runs from 2000 through 2100.*

Ozone production is expected to be in the so-called ÒNMVOC limited rangeÓ (Duncan and Chameides, 1998; Sillman, 1999) in most urban areas. Therefore, an increase in NO_x mole fractions should not necessarily lead to higher ozone concentrations. A scatter plot of 24-hour

and domain average NO_x and NMVOC mole fractions versus 1-hour peak ozone mole fraction is shown in **Figure 16** for both the META and META-TIME runs for the data obtained from 1990 through 2100. NO_x, NMVOC and O_3 mole fractions are the average of the three types of urban areas but not the average of several latitudinal bands. Although in the META run, both NO_x and NMVOC emissions in cities grow over time, the NO_x mole fraction is decreasing (see also Fig. 13) where at the same time the NMVOC mole fraction is increasing. The peak ozone is found to be higher with higher NMVOC mole fractions. In the META-TIME run the NO_x mole fractions vary considerably (see Fig. 13) but the ozone mole fractions are altered little, due to the quasi-constant NMVOC mole fractions. These results suggest that the urban atmospheric chemistry predicted by our model is indeed within the NMVOC limited regime.

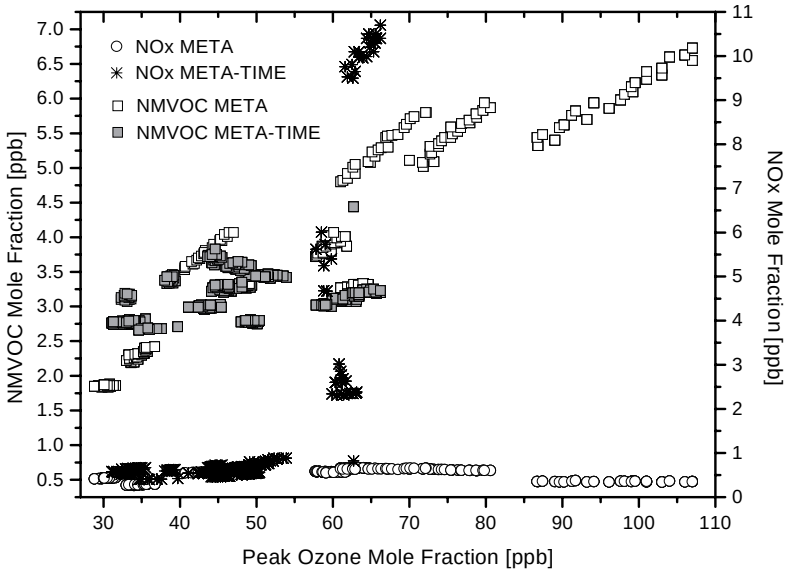

***Figure 16**. Annual average NO_x and NMVOC mole fractions in urban domains versus peak ozone mole fraction for the META and META-TIME. For the definition of several mole fractions see text. This analysis suggests that the ozone production in the urban areas is NMVOC limited.*

5.3 CO

The CO fluxes from cities increase substantially in the META-TIME run, while they grow only little in the META run. The CO mole fractions increase in both runs, although more so in the META run. In **Figure 17** we plot the fluxes and daily average surface mole fractions over the urban domains for the two simulations. Fluxes and mole fractions are the global average of all three types of urban areas.

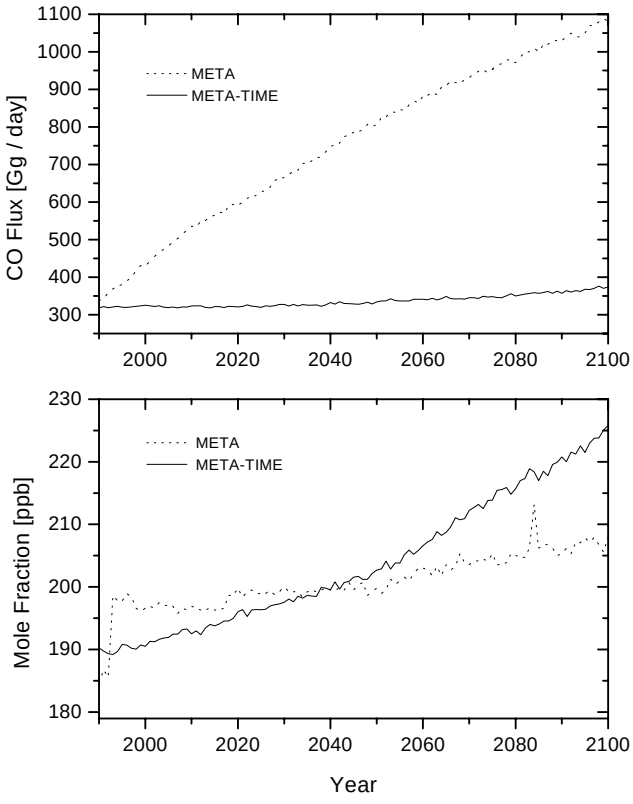

***Figure 17**. Annual average CO fluxes exported from urban domains and surface mole fractions in the urban domains for the META and META-TIME runs for 1990 to 2100. For definition of the CO flux and mole fraction see text.*

5.4 Discussion

Allocating urban emissions as in the META and META-TIME runs provides two extreme scenarios for emissions strengths in urban areas. In the META-TIME run, conversion of NO_x to NO_y proves to be much more efficient than in the META run; therefore, less NO_x is available to the rural areas on a global scale. **Table 5** lists the ratios of NO_y to NO_x for the two runs in 2000, 2050, and 2100, for both fluxes (moles/time) from and moles within the urban domains. To facilitate calculation of the ratio NO_y to NO_x, we express all nitrogen-containing species in terms of their nitrogen content. The more NO_x is converted to NO_y, the higher is the value of the ratio derived. In the META-TIME run, the NO_y to NO_x ratio of moles declines over time, due to a relative increase in the number of medium and highly polluted cities with higher NO_x emissions in 2050 and 2100, compared to the initial distribution in 1990.

***Table 5**. Ratio of NO_y to NO_x fluxes (moles/time) out of the urban domains and the ratio of NO_y to NO_x moles within the urban domains derived for the cases META-TIME and META for the years 2000, 2050, and 2100.*

	META-TIME		META	
Year	**Fluxes**	**Moles**	**Fluxes**	**Moles**
2000	2.7	5.4	2.1	1.2
2050	3.1	2.1	1.8	1.2
2100	2.7	1.9	1.7	1.3

Global as opposed to urban tropospheric ozone mole fractions are basically determined by the available NO_x. Although we produce more ozone in urban domains when implementing the urban chemistry model, the global tropospheric ozone mole fraction is lower in the two META cases than in the reference case because of lower global NO_x mole fractions. In both runs with the urban chemistry model the effective total NO_x emissions (rural emissions plus flux of NO_x out of urban areas) to the global model are lower than in the reference case. This is primarily due to the efficient conversion of NO_x to HNO_3 and N_2O_5 (NO_2 and HNO_3 fluxes are roughly the same, see Fig. 14) in urban areas, where both species are sinks for NO_x. At the low average NO_x mole fractions (< 1 ppb) predicted by the global model, changes of NO_x are not expected to alter the ozone production per unit NO_x per day (*e.g.*, Liu *et al.*, 1987) and ozone should follow proportionally the NO_x trend (in our case about 7% decrease in NO_x and O_3). Ozone is one of the main factors determining OH, and therefore with lower O_3 mole fractions we observe also lower OH concentrations (note that other factors influencing OH concentration such as CO, CH_4, and water vapor content or radiation do change over time but have a relatively smaller effect).

This suggests that, without considering the highly nonlinear chemistry in urban areas, global-scale models will most likely overestimate tropospheric ozone production due to unreasonably high background NO_x concentrations. Several investigators (*e.g.*, Duncan and Chameides, 1998; Roselle and Schere, 1995; Chameides *et al.*, 1992; Sillman *et al.*, 1990; Lin *et al.*, 1988) have addressed this latter issue and came to the same conclusion. Our contribution is the introduction of a computationally efficient and accurate parameterization of urban chemistry which allows quantitative estimation of the effects of urban versus rural emissions in a global model, Note also, that by adding the reduced-form urban model to our global 2D model, a substantial amount of the total NO_x emissions are processed more reasonably. As a result the distribution of the remaining rural NO_x emissions should have a significantly smaller latitudinal gradient. Under

this circumstance, the difference between a 2D and a 3D global model should be lessened, assuming that urban emissions are treated properly in our 3D urban (CIT) model. Compared to the reference run, the global tropospheric CO mole fraction does not change substantially through urban chemistry, in the first half of our simulation for the META and META-TIME runs, despite an additional CO source from NMVOC emissions. This slight reduction is attributed to the very efficient CO oxidation in urban areas, which are characterized by relatively high OH concentrations. As a result, less CO is emitted to the global troposphere. After 2050, the global CO mole fraction in the META-TIME run is higher than in the reference run. Urban CO fluxes from the urban domains grow over time not only because of an increase in the number of cities, but also because of the relative growth in urban CO and NMVOC emissions. Therefore, more CO is released from urban to rural areas in the global model. At the same time, the global OH concentration falls constantly, and the methane mole fraction increases constantly. Both factors (the increasing fluxes and the increasing lifetime of CO) lead eventually to higher global CO mole fractions (*e.g.*, Wang and Prinn, 1999).

6. SUMMARY

We have derived a "reduced-form" model or "parameterization" for urban air chemistry based on the California Institute of Technology–Carnegie Institute of Technology (at Carnegie Mellon University) Urban Airshed Model by employing the probabilistic collocation method. The reduced-form model is computationally efficient and in good agreement with the parent urban airshed model over a wide range of input parameters. Incorporating this reduced-form model into the MIT 2D-LO coupled chemistry-climate model enables us to quantify the impact of urban air pollution on global chemistry and climate. By linking an urban airshed model to the 2D-LO global coupled chemistry-climate model we incorporated a high resolution 3D model with complex NMVOC chemistry into a computationally efficient global model with O_3-HO_x-NO_x-CO-CH_4 background chemistry coupled to a climate model. Based on our definition of urban areas up to 50% of NO_x, CO, and NMVOC emissions originate from these regions. The remaining rural emissions are now expected to be more evenly distributed, in which case the average features of the 2D model should be a more reasonable approximation compared to the earlier approach. We expect the use of alternative global scale models to ours will lead to qualitatively if not quantitatively similar results.

Three simulations, each including or excluding the reduced-form model, have been carried out for the time period from 1977 to 2100 using identical emissions data. In the two runs involving the reduced-form model, urban emissions of NO_x, NMVOC, CO, and SO_x are allocated in different ways. In one run, the number of cities and the proportions of urban versus rural emissions have 1990 values, which leads to a steady increase in emissions per city. In the other run, we increase the number of polluted urban areas and the partitioning of urban and rural emissions, so that emissions urban area are constant over time. These two simulations are compared to the reference, which does not utilize the reduced-form model.

We have found that the efficient conversion of NO_x to NO_y, especially to PAN and to HNO_3, in urban areas leads to lower global tropospheric NO_x concentrations than in the reference (5% to 10% lower in 2100). As a result, the tropospheric mole fraction of ozone and the OH free radical concentration decrease relative to the reference (in 2100, O_3 5% to 7% lower, and OH 3% to 7% lower), as well. The tropospheric mole fraction of CH_4 increases relative to the reference (in 2100, 7% to 11% higher) as a result to the lower OH concentration. The tropospheric CO mole fraction is altered up or slightly down due to urban chemistry, with the amount depending on the assumptions used for urban emissions. The effect on global mean surface temperature of implementing the reduced-form urban model is not however large because the decrease in radiative forcing by ozone is offset approximately by the increase in radiative forcing by CH_4. We are currently preparing to include aged emissions of PAN produced in urban areas into the global coupled chemistry-climate model, which could lead to slightly higher global NO_x concentrations than the current results suggest.

Acknowledgements. We thank several MIT colleagues: Gary Adamkiewicz and Gregory McRae who helped with the CIT model, Jean Fitzmaurice who provided support with emissions calculations, and Judith Stitt who helped edit the manuscript. We also thank Josep Calbo (Universitat de Girona) for assistance regarding the parameterization of the CIT model. This research was supported through an Erwin Schr dinger Fellowship awarded by the Austrian Science Fund (J1527-GEO) to MM, by the National Science Foundation (grants ATM-9523616 and ATM-9610145), by the Department of Energy (grants DE-FGO2-94ER61937 and DE-FGO2-93ER61713), and by MITÕs Joint Program on the Science and Policy of Global Change, which is supported by a number of industrial and government sponsors.

REFERENCES

Atkinson, R., Gas-phase tropospheric chemistry of organic compounds: a review, *Atmos. Environ.*, 24A, 1-41, 1990.

Atkinson, P.S., D.L. Baulch, R.A. Cox, R.S. Hampson, Jr., J.A. Kerr, and J. Troe, Evaluated kinetic and photochemical data for atmospheric chemistry, *J. Phys. Chem. Ref. Data*, 21, 1125-1444, 1992.

Brasseur, G., J.-F. Muller, and C. Granier, Atmospheric impact of NO_x emissions by subsonic aircraft: A three-dimensional model study, *J. Geophys. Res.*, 101, 1423–28, 1996.

Bouscaren, R., *Inventaire des Emissions de Pollutants dans LÕAtmosphere dans La Communate Europeenne en 1985*, Centre Interprofessionel Technique dÕEtude de la Pollution Atmosph rique (CITEPA), 1990.

Calbo, J., W. Pan, M. Webster, R. Prinn, and G.J. McRae, Parameterization of urban subgrid scale processes in global atmospheric chemistry models, *J. Geophys. Res.*, 103, 3437-51, 1998.

Carnovale, F., P. Alviano, C. Carvalho, G. Deitch, S. Jiang, D. Macaulay, and M. Summers, Air emissions inventory for the Port Phillip Control Region, *Clean Air*, 26, 134-44, 1992.

Carter, W.P.L., A detailed mechanism for the gas-phase atmospheric reactions of organic compounds, *Atmos. Environ.*, 24A, 481-518, 1990.

Chameides, W.L., F. Fehsenfeld, M.O. Rodgers, C. Cardelino, J. Martinez, D. Parrish, W. Lonneman, D.R. Lawson, R.A. Rasmussen, P. Zimmerman, J. Greenberg, P. Middleton, and T. Wang, Ozone precursor relationships in the ambient atmosphere, *J. Geophys. Res.*, 97, 6037-6055, 1992.

Crutzen, P.J., and P.H. Zimmermann, The changing photochemistry of the troposphere, *Tellus*, 43AB, 136-151, 1991.

DeMore, W.B., S.P. Sander, D.M. Golden, R.F. Hampson, M.J. Kurylo, C.J. Howard, A.R. Ravishankara, C.E. Kolb, and M.J. Molina, Chemical kinetics and photochemical data for use in stratospheric modeling: Evaluation number 11, *JPL Publ. Rep*. 94-26, 1994.

Dignon, J., NO_x and SO_x Emissions from fossil fuels: A global distribution, *Atmos. Environ*., 26A, 1157-1163, 1992.

Duncan, B.N., and W.L. Chameides, Effects of urban emission control strategies on the export of ozone and ozone precursors from the urban atmosphere to the troposphere, *J. Geophys. Res*., 103, 28,159-28,179, 1998.

EPA, *National air pollutant emission trends, 1990-1996*, United States Environmental Protection Agency, Office of Air Quality Planning and Standards, Research Triangle Park, NC, *EPA-454/R-097-011*, 1997.

Finlayson-Pitts, B.J., and J.N. Pitts, *Atmospheric Chemistry: Fundamentals and Experimental Techniques*, 1098 pp., John Wiley & Sons, New York, 1986.

Fung, I., J. John, J. Lerner, E. Matthews, M. Prather, L.P. Steele, and P.J. Fraser, Three-dimensional model synthesis of the global methane cycle, *J. Geophys. Res*., 96, 13,003-13,065, 1991.

Harley, R.A., A.G. Russell, G.J. McRae, G.R. Cass, and J.H. Seinfeld, Photochemical modeling of the Southern Californian Air Quality Study, *Environ. Sci. Technol.*, 27, 378-388, 1993.

Hauglustaine, D., and C. Granier, Radiative forcing by tropospheric ozone changes due to increased emissions of CH_4, CO, and NO_x, in: *Atmospheric Ozone as a Climate Gas*, edited by W. Wang and I. Isaksen, NATO ASI Ser., 32, 1995.

Jacob, D.J., Chemistry of OH in remote clouds and its role in the production of formic acid and peroxymonosulfate, *J. Geophys. Res*., 91, 9807-9826, 1986.

Japar, S.M., T.J. Wallington, J.F.O. Richert, J.C. Ball, The atmospheric chemistry of oxygenated fuel additives – tert-butyl alcohol, dimethyl ether, and methyl tert-butyl ether, *Int. J. Chem. Kinet*., 22, 1257-1269, 1990.

Kato, N., and H. Akimoto, Anthropogenic Emissions of SO_2 and NO_x in Asia: Emissions Inventories (plus errata), *Atmos. Environ*., 26A, 2997-3017, 1992.

Levy, H., Photochemistry of the lower troposphere, *Planet. Space Sci*., 20, 919-35, 1972.

Lin, X., M. Trainer, and S.C. Liu, On the nonlinearity of the tropospheric ozone production, *J. Geophys. Res*., 93, 15,879-15,888, 1988.

Lind, J.A., and G.L. Kok, Henry's law determinations for aqueous solutions of hydrogen peroxide, methylhydroperoxide, and peroxyacetic acid, *J. Geophys. Res*., 91, 7889-7895, 1988.

Liu, S.C., M. Trainer, F.C. Fehsenfeld, D.D. Parrish, E.J. Williams, D.W. Fahey, G. H bler, and P.C. Murphy, Ozone production in the rural troposphere and the implications for regional and global ozone distributions, *J. Geophys. Res*., 92, 4191-4207, 1987.

Long-range World Population Projections, Two Centuries of Population Growth 1950 – 2150, United Nations, New York, 1992.

Lurmann, F.W., W.P.L. Carter, and L.A. Coyner, A surrogate species chemical mechanism for urban-scale air quality simulation models, United States Environmental Protection Agency, *EPA/600/3-87/014a* and *EPA/600/3-87/014b*, 1987.

McRae, G.J., et al., Development of a second generation mathematical model of urban air pollution, I, Model formulation, *Atmos. Environ.*, 16, 679-696, 1982.

Olivier, J.G.J., A.F. Bouwmann, C.W.M. van der Mass, J.J.M. Berdowski, C. Veldt, J.P.J. Bloos, A.J.H. Visschedijk, P.Y.J. Zandveld, and J.L. Haverlag, Description of EDGAR Version 2.0: A set of global emission inventories of greenhouse gases and ozone depleting substances for all anthropogenic and most natural sources on a per country basis and on 1¡ × 1¡ grid, *Report no. 771060002. RIVM*, Bilthoven, 1995.

Pandis, S.N., and J.H. Seinfeld, Sensitivity analysis of a chemical mechanism for aqueous-phase atmospheric chemistry, *J. Geophys. Res.*, 94, 1105-1126, 1989.

Perrin, D.D., *Ionization Constants of Inorganic Acids and Bases in Aqueous Solution*, 2nd ed., Pergamon Press, New York, 1982.

Pickering, K., *et al*., Convective transport of biomass burning emissions over Brazil during TRACE A, *J. Geophys. Res.*, 101, 23,993-24,012, 1996.

Prinn, R.G., R.F. Weiss, B.R. Miller, J. Huang, F.N. Alyea, D.M. Cunnold, P.J. Fraser, D.E. Hartley, and P.G. Simmonds, Atmospheric trends and lifetime of CH_3CCl_3 and global OH concentrations, *Science*, 269, 187-192, 1995.

Prinn, R., H. Jacoby, A. Sokolov, C. Wang, X. Xiao, Z. Yang, R Eckhaus, P. Stone, D. Ellerman, J. Melillo, J. Fitzmaurice, D. Kicklighter, G. Holian, and Y. Liu, Integrated global system model for climate policy assessment: Feedbacks and sensitivity studies, *Climatic Change*, 41, 469-546, 1999.

Reilly, J., R. Prinn, J. Harnisch, J. Fitzmaurice, H. Jacoby, D. Kicklighter, J. Melillo, P. Stone, A. Sokolov, and C. Wang, Multi-gas assessment of the Kyoto Protocol, *Nature*, 401, 549-555, 1999.

Roselle, S.J., and K.L Schere, Modeled response of photochemical oxidants to systematic reduction in anthropogenic volatile organic compound and NO_x emissions, *J. Geophys. Res.*, 100, 22,929-22,941, 1995.

Saeger, M., J. Langstaff, R. Walters, L. Modica, D. Zimmerman, D. Fratt, D. Dulleba, R. Ryan, J. Demmy, W. Tax, D. Sprague, D. Mudgett, and A.S. Werner, The 1985 NAPAP Emissions Inventory (Version 2): Development of the Annual Data and ModelersÕ Tapes, U.S. Environ. Protection Agency, Research Triangle Park, NC, *Rep. EPA-600/7-89-012a*, 1989.

Sandnes, H., and H. Styve, *Calculated Budgets for Airborne Acidifying Components in Europe, 1985, 1986, 1987, 1988, 1989, 1990, and 1991*, Meteorological Synthesizing Center - West. The Norwegian Meteorological Institute, Oslo, Norway, 1992.

Schwartz, S.E., Gas- and aqueous-phase chemistry of HO_2 in liquid water clouds, *J. Geophys. Res.*, 89, 11,589-11,598, 1984.

Seinfeld, J.H., and S.N. Pandis, *Atmospheric chemistry and physics: From air pollution to climate change*, pp. 299-302, John Wiley, New York, 1998.

Sillman, S., J.A. Logan, S.C. Wofsy, A regional scale model for ozone in the United States with subgrid representation of urban and power plant plumes, *J. Geophys. Res.*, 95, 5731-5748, 1990.

Sillman, S., The relation between ozone, NO_x and hydrocarbons in urban and polluted rural environments, *Atmos. Environ.*, 33, 1821-1845, 1999.

Smith, R.M., and A.E. Martell, *Critical Stability Constants, Volume 4: Inorganic Complexes*, Plenum Press, New York, 1976.

Sokolov, A.P., and P.H. Stone, A flexible climate model for use in integrated assessments, *Climate Dynamics*, 14, 291-303, 1998.

Spiro, P.A., D.J. Jacob, and J.A. Logan, Global inventory of sulfur emissions with a 1¡ × 1¡ resolution, *J. Geophys. Res*., 97, 6023-6036, 1992.

Stockwell, W.R., On the $HO_2 + HO_2$ reaction: Its misapplication in atmospheric chemistry models, *J. Geophys. Res.*, 100, 11,695-11,698, 1995.

Tatang, M.A., W.W. Pan, R.G. Prinn, G.J. McRae, An efficient method for parametric uncertainty analysis of numerical geophysical models, *J. Geophys. Res.*, 102, 925-932, 1997.

Urban Air Pollution in Megacities of the World, WHO and UNEP, Blackwell Publishers, Oxford, 1992.

Wagner, J., R.A. Walters, L.J. Maiocco, and D.R. Neal, *Development of the 1980 NAPAP Emissions Inventory*, U.S. Environmental Protection Agency, Washington, DC, 1986.

Wang, C., R.G. Prinn, and A.P. Sokolov, A global interactive chemistry and climate model: Formulation and testing, *J. Geophys. Res.*, 103, 3399-3417, 1998.

Wang, C., and R.G. Prinn, Impact of emissions, chemistry and climate on atmospheric carbon monoxide: 100-yr predictions from a global chemistry-climate model, *Chemosphere*, 1, 73-81, 1999.

Wang, W., D. Wuebbles, W. Washington, R. Isaacs, and G. Molnar, Trace gases and other potential perturbations to global climate, *Rev. Geophysics*., 24 (1): 110-140, 1986.

World Recourses, *A Guide to the Global Environment, The Urban Environment 1996-1997*, Oxford University Press, 1996.

World Urbanization Prospects, The 1996 Revision, United Nations, New York, 1998.

Xiao, X., D.W. Kicklighter, J.M. Melillo, A.D. McGuire, P.H. Stone, A.P. Sokolov, Linking a global terrestrial biogeochemical model and a 2-dimensional climate model: Implications for the global carbon budget, *Tellus*, B 49, 18-37, 1997.

Xiao, X., J.M. Melillo, D.W. Kicklighter, A.D. McGuire, R.G.Prinn, C. Wang, P.H. Stone, and A. Sokolov, Transient climate change and net ecosystem production of the terrestrial biosphere, *Global Biogeochem. Cycles*, 12 (2): 345-360, 1998.

Yang, M.S., R.S. Eckaus, A.D. Ellerman, H.D. Jacoby, The MIT Emissions Prediction and Policy Analysis (EPPA) Model, MIT Joint Program on the Science and Policy of Global Change, *Report No. 6*, 49 pp., 1996.

APPENDIX

CIT Species and Reactions

Abbreviation	Species name	Abbreviation	Species name
NO	nitric oxide	NPHE	nitrophenols
NO_2	nitrogen dioxide	NH3	ammonia
O_3	ozone	NIT	aerosol nitrate
HONO	nitrous acid	MEOH	methanol
HNO_3	nitric acid	ETOH	ethanol
HNO_4	pernitric acid	MTBE	methyl tert-butyl ether
N_2O_5	nitrogen pentoxide	OSD	O singlet D
NO_3	nitrate radical	O	O atom
HO_2	hydroperoxy radical	OH	hydroxyl radical
CO	carbon monoxide	RO_2R	general RO_2 #1
HCHO	formaldehyde	R_2O_2	general RO_2 #2
ALD2	lumped aldehydes	RO_2N	alkyl nitrate RO_2
MEK	methyl ethyl ketone	RO_2P	phenol RO_2
MGLY	methylglyoxyl	BZN2	benzaldehyde N-RO_2
PAN	peroxyl acyl nitrate	BZO	phenoxy radical
RO_2	total RO_2 radicals	ISOP	isoprene
MCO_3	CH_3CO_3 radical	H_2O_2	hydrogen peroxide
ALKN	alkyl nitrate	H_2O	water vapor
ALKA	>C3 alkanes	O_2	oxygen
ETHE	ethene	H_2	hydrogen
ALKE	>C2 alkenes	SO_2	sulfur dioxide
TOLU	toluene	SO_3	sulfur trioxide
AROM	aromatics	M	third body
DIAL	unknown dicarbonyls	TBF	tert-butyl formate, treated as inert species

Gas phase chemical reaction included in the CIT model

Reaction		Rate Constant	Ref.
R1	$NO_2 + h\nu \rightarrow NO + O$	radiation dependent	1
R2	$O + O_2 + M \rightarrow O_3 + M$	$1.05 \times 10^{4}\ e^{1282/T}$	1
R3	$O + NO_2 \rightarrow NO + O_2$	9.3×10^{-12}	1
R4	$O + NO_2 + M \rightarrow NO_3 + M$	$1.11 \times 10^{-13}\ e^{894/T}$	1
R5	$NO + O_3 \rightarrow NO_2$	$1.8 \times 10^{-12}\ e^{-1370/T}$	1
R6	$NO_2 + O_3 \rightarrow NO_3$	$1.2 \times 10^{-13}\ e^{-2450/T}$	1
R7	$NO + NO_3 \rightarrow 2\ NO_2$	$8 \times 10^{-12}\ e^{252/T}$	1
R8	$NO + NO \rightarrow 2\ NO_2$	$1.64 \times 10^{-20}\ e^{529/T}$	1
R9	$NO_2 + NO_3 + M \rightarrow N_2O_5 + M$	$4.62 \times 10^{-13}\ e^{273/T}$	1
R10	$N_2O_5 \rightarrow NO_2 + NO_3$	$1.33 \times 10^{15}\ e^{-11379/T}$	1
R11	$N_2O_5 + H_2O \rightarrow 2\ HNO_3$	1×10^{-21}	1
R12	$NO_2 + NO_3 \rightarrow NO + NO_2$	$2.5 \times 10^{-14}\ e^{-1229/T}$	1
R13	$NO_3 + h\nu \rightarrow NO$	radiation dependent	1
R14	$NO_3 + h\nu \rightarrow NO_2 + O$	radiation dependent	1
R15	$O_3 + h\nu \rightarrow O$	radiation dependent	1
R16	$O_3 + h\nu \rightarrow OSD$	radiation dependent	1
R17	$OSD + H_2O \rightarrow 2\ OH$	2.2×10^{-10}	1
R18	$OSD \rightarrow O$	7.2×10^{8}	1
R19	$NO + OH + M \rightarrow HONO + M$	$4.03 \times 10^{-13}\ e^{833/T}$	1
R20	$HONO + h\nu \rightarrow NO + OH$	radiation dependent	1
R21	$NO_2 + H_2O \rightarrow HONO - NO_2 + HNO_3$	4×10^{-24}	1
R22	$NO_2 + OH + M \rightarrow HNO_3 + M$	$9.58 \times 10^{-13}\ e^{737/T}$	1
R23	$HNO_3 + OH \rightarrow NO_3$	$9.4 \times 10^{-15}\ e^{778/T}$	1
R24	$CO + OH \rightarrow HO_2$	2.18×10^{-13}	1
R25	$O_3 + OH \rightarrow HO_2$	$1.6 \times 10^{-12}\ e^{-942/T}$	1
R26	$NO + HO_2 \rightarrow NO_2 + OH$	$3.7 \times 10^{-12}\ e^{240/T}$	1
R27	$NO_2 + HO_2 \rightarrow HNO_4$	$1.02 \times 10^{-13}\ e^{773/T}$	1
R28	$HNO_4 \rightarrow NO_2 + HO_2$	$4.35 \times 10^{13}\ e^{-10103/T}$	1
R29	$HNO_4 + OH \rightarrow NO_2$	4×10^{-12}	1
R30	$O_3 + HO_2 \rightarrow OH$	$1.4 \times 10^{-14}\ e^{-579/T}$	1
R31	$HO_2 + HO_2 \rightarrow H_2O_2$	$2.27 \times 10^{-13}\ e^{771/T}$	1
R32	$HO_2 + HO_2 + H_2O \rightarrow H_2O_2$	$3.26 \times 10^{-34}\ e^{2971/T}$	1
R33	$NO_3 + HO_2 \rightarrow HNO_3$	$2.27 \times 10^{-13}\ e^{771/T}$	1
R34	$NO_3 + HO_2 + H_2O \rightarrow HNO_3$	$3.26 \times 10^{-34}\ e^{2971/T}$	1
R35	$RO_2 + NO \rightarrow NO$	$4.2 \times 10^{-12}\ e^{180/T}$	1
R36	$RO_2 + HO_2 \rightarrow HO_2$	3×10^{-12}	1
R37	$RO_2 + RO_2 \rightarrow$ products	1×10^{-15}	1
R38	$RO_2 + MCO_3 \rightarrow$ products	3×10^{-12}	1
R39	$HCHO + h\nu \rightarrow 2\ HO_2 + CO$	radiation dependent	1
R40	$HCHO + h\nu \rightarrow CO$	radiation dependent	1
R41	$HCHO + OH \rightarrow HO_2 + CO$	9×10^{-12}	1
R42	$HCHO + NO_3 \rightarrow HNO_3 + HO_2 + CO$	$6 \times 10^{-13}\ e^{-2060/T}$	1
R43	$HCHO + HO_2 \rightarrow RO_2R + RO_2$	1×10^{-14}	1

Reaction	[continued]	Rate Constant	Ref.
R44	ALD2 + OH → MCO_3	$6.9 \times 10^{-12}\ e^{250/T}$	1
R45	ALD2 + hν → CO + HCHO + RO_2R + HO_2C + RO_2	radiation dependent	1
R46	ALD2 + NO_3 → HNO_3 + MCO_3	$3 \times 10^{-13}\ e^{-1427/T}$	1
R47	MCO_3 + NO → NO_2 + HCHO + RO_2R + RO_2	$4.2 \times 10^{-12}\ e^{180/T}$	1
R48	MCO_3 + NO_2 → PAN	$2.8 \times 10^{-12}\ e^{180/T}$	1
R49	MCO_3 + HO_2 → HCHO	3×10^{-12}	1
R50	MCO_3 + MCO_3 → 2 HO_2 + 2 HCHO	2.5×10^{-12}	1
R51	PAN → MCO_3 + NO_2	$2 \times 10^{16}\ e^{-13542/T}$	1
R52	MEK + hν → MCO_3 + ALD2 + RO_2R + RO_2	radiation dependent	1
R53	MEK + OH → 1.2 R_2O_2 + 1.2 RO_2 + MCO_3 + 0.5 ALD2 + 0.5 HCHO	$1.2 \times 10^{-11}\ e^{-745/T}$	1
R54	MGLY + hν → MCO_3 + HO_2 + CO	radiation dependent	1
R55	MGLY + OH → MCO_3 + CO	1.7×10^{-11}	1
R56	MGLY + NO_3 → HNO_3 + MCO_3 + CO	$3 \times 10^{-13}\ e^{-1427/T}$	1
R57	ALKA + OH → B1 HCHO + B2 ALD2 + B3 MEK + B4 RO_2N + B6 R_2O_2 + B7 RO_2	$1.053 \times 10^{-11}\ e^{-354/T}$ X + $1.62 \times 10^{-11}\ e^{-289/T}$(1-X)	1[a,b]
R58	ALKN + OH → NO_2 + 0.15 MEK + 1.53 ALD2 + 0.16 HCHO + 1.39 R_2O_2 + 1.39 RO_2	$2.19 \times 10^{-11}\ e^{-709/T}$	1
R59	RO_2N + NO → ALKN	$4.2 \times 10^{-12}\ e^{180/T}$	1
R60	RO_2N + HO_2 → MEK	3×10^{-12}	1
R61	RO_2N + RO_2 → RO_2 + HO_2 + MEK	1×10^{-15}	1
R62	RO_2N + MCO_3 → HCHO + HO_2 + MEK	3×10^{-12}	1
R63	R_2O_2 + NO → NO_2	$4.2 \times 10^{-12}\ e^{180/T}$	1
R64	R_2O_2 + HO_2 → products	3×10^{-12}	1
R65	R_2O_2 + RO_2 → RO_2	1×10^{-15}	1
R66	R_2O_2 + MCO_3 → HCHO + HO_2	3×10^{-12}	1
R67	RO_2R + NO → NO_2 + HO_2	$4.2 \times 10^{-12}\ e^{180/T}$	1
R68	RO_2R + HO_2 → products	3×10^{-12}	1
R69	RO_2R + RO_2 → 0.5 HO_2 + RO2	1×10^{-15}	1
R70	RO_2R + MCO_3 → HO_2 + HCHO	3×10^{-12}	1
R71	ETHE + OH → RO_2R + RO_2 + 1.56 HCHO + 0.22 ALD2	$2.15 \times 10^{-12}\ e^{411/T}$	1
R72	ETHE + O_3 → HCHO + 0.12 HO_2 + 0.42 CO	$1.2 \times 10^{-14}\ e^{-2634/T}$	1
R73	ETHE + O → RO_2R + RO_2 + CO + HCHO + HO_2	$1.04 \times 10^{-11}\ e^{-792/T}$	1
R74	ETHE + NO_3 → RO_2 + NO_2 + 2 HCHO + R_2O_2	$2 \times 10^{-12}\ e^{-2925/T}$	1
R75	ALKE + OH → RO_2 + RO_2 + B8 HCHO + B9 ALD2	$4.85 \times 10^{-12}\ e^{504/T}$ Y + $1.01 \times 10^{-11}\ e^{549/T}$ (1-Y)	1[a, c]
R76	ALKE + O_3 → B10 HCHO + B11 ALD2 + B12 RO_2R + B12 RO_2 + B13 HO_2 + B14 OH + B15 CO	$1.32 \times 10^{-4}\ e^{-2105/T}$ Y + $9.08 \times 10^{-15}\ e^{-1137/T}$ (1-Y)	1[a, c]
R77	ALKE + O → B16 CO + B17 MEK + B18 HCHO + B19 ALD2 + B20 HO_2 + B21 RO_2R + B21 RO_2	$1.18 \times 10^{-11}\ e^{-324/T}$ Y + $2.26 \times 10^{-11}\ e^{10/T}$ (1-Y)	1[a, c]
R78	ALKE + NO_3 → NO_2 + B8 HCHO + B9 ALD2 + R_2O_2 + RO_2	$5 \times 10^{-12}\ e^{-1935/T}$ + $1 \times 10^{-11}\ e^{-975/T}$ (1-Y)	1[a, c]
R79	TOLU + OH → 0.16(CRES + HO_2) + 0.4 DIAL + 0.84 RO_2 + 0.144 MGLY + 0.11 HCHO + 0.114 CO + 0.84 RO_2R	$2.1 \times 10^{-12}\ e^{322/T}$	1

Reaction	[continued]	Rate Constant	Ref.
R80	AROM + OH → 0.17 CRES + 0.17 HO_2 + 0.83 RO_2R + 0.83 RO_2 + B22 DIAL + B23 MGLY + B24 CO	$1.66 \times 10^{-11}\ e^{116/T}$ Z + 6.2×10^{-11} (1-Z)	1[a, d]
R81	DIAL + OH → MCO_3	3×10^{-11}	1
R82	DIAL + hν → HO_2 + CO + MCO_3	radiation dependent	1
R83	CRES + OH → 0.2 MGLY + 0.15 RO_2P + 0.85 RO_2R + RO_2	4×10^{-11}	1
R84	CRES + NO_3 → HNO_3 + BZO	2.2×10^{-11}	1
R85	RO_2P + NO → NPHE	$4.2 \times 10^{-12}\ e^{180/T}$	1
R86	RO_2P + HO_2 → products	3×10^{-12}	1
R87	RO_2P + RO_2 → 0.5 HO_2 + RO_2	1×10^{-15}	1
R88	RO_2P + MCO_3 → HCHO + HO_2	3×10^{-12}	1
R89	BZO + NO_2 → NPHE	1.5×10^{-11}	1
R90	BZO + HO_2 → products	3×10^{-12}	1
R91	BZO → products	1×10^{-3}	1
R92	NPHE + NO_3 → HNO_3 + BZN_2	3.8×10^{-12}	1
R93	BZN_2 + NO_2 → products	1.5×10^{-11}	1
R94	BZN_2 + HO2 → NPHE	3×10^{-12}	1
R95	BZN_2 → NPHE	1×10^{-3}	1
R96	H_2O_2 + hν → 2 OH	radiation dependent	1[e]
R97	H_2O_2 + OH → HO_2	$3.1 \times 10^{-12}\ e^{-187/T}$	1[e]
R98	MEOH + OH → HCHO + HO_2	$5.75 \times 10^{-13}\ T^2\ e^{148/T}$	2
R99	CH_4 + OH → HCHO + RO_2 + RO_2R	$6.95 \times 10^{-18}\ T^2\ e^{-1282/T}$	2
R100	ISOP + OH → HCHO + ALD2 + RO_2R + RO_2	$2.54 \times 10^{-11}\ e^{410/T}$	2
R101	ISOP + O_3 → 0.5 HCHO + 0.65 ALD2 + 0.21 MEK + 0.16 HO_2 + 0.29 CO + 0.06 OH + 0.14 (RO_2R + RO_2)	$1.23 \times 10^{-14}\ e^{-2013/T}$	2
R102	ISOP + O → 0.4 HO_2 + 0.5 MEK + 0.5 ALD2	6×10^{-11}	2
R103	ISOP + NO_3 → NO_2 + HCHO + ALD2 + R_2O_2 + RO_2	$2.54 \times 10^{-11}\ e^{-1121/T}$	2
R104	ETOH + OH → ALD2 + HO_2	$5.56 \times 10^{-13}\ T^2\ e^{532/T}$	2
R105	MTBE + 1.4 OH → 0.6 TBF + 0.4 HCHO + 0.4 MEK + 1.4 RO_2R + 0.4 R_2O_2 + 1.8 RO_2	$6.82 \times 10^{-18}\ T^2\ e^{460/T}$	3, 4
R106	SO_2 + OH → SO_3 + HO_2	9.1×10^{-13}	2

Notes: Rate constants given in cm^3 $molecule^{-1}$ s^{-1}; T in Kelvin.

[a] B_i in reaction 57, 75, 76, 77, 78, and 80 are pressure and temperature dependent stochiometric coefficients of the condensed LCC mechanism; for details, see Lurmann *et al*., 1987

[b] X is the ratio of C4-C5 alkanes to >C3 alkanes on a mole basis, see Lurmann *et al*., 1987

[c] Y is the ratio of terminal alkenes to >C2 alkenes on a mole basis, see Lurmann *et al*., 1987

[d] Z is the ratio of di-alkylbenzenes to di- and tri-alkylbenzenes on a mole basis, see Lurmann *et al*., 1987

[e] OZIPM mechanism is another condensed mechanism of the LCC formulation intended for use in Ozone Isopleth Plotting Package with Optional mechanisms (OZIPM), see Lurmann *et al*., 1987

References: 1) Lurmann *et al*., 1987; condensed LCC mechanism; 2) Carter, 1990; 3) Japar *et al*., 1990; 4) Atkinson, 1990

Gaseous phase chemical reactions included in the global chemistry-climate model

Reaction		A, k_0, or k_∞	-E/R or f(T)	Ref.
R1	$O_3 + h\nu \rightarrow O(^1D) + O_2$			1
R2	$O(^1D) + H_2O \rightarrow 2OH$	2.2×10^{-10}	-	1
R3	$O(^1D) + N_2 \rightarrow O + N_2$	1.8×10^{-11}	107	1
R4	$O(^1D) + O_2 \rightarrow O + O_2$	3.2×10^{-11}	67	1
R5	$CO + OH \rightarrow H + CO_2$	1.5×10^{-13} [1 + 0.6 p(atm)]	-	1
R6	$H + O_2 + M \rightarrow HO_2 + M$	$k_0 = 6.2 \times 10^{-32}$	$(T/300)^{-1.6}$	2
		$k_\infty = 7.5 \times 10^{-11}$	-	2
R7	$HO_2 + NO \rightarrow OH + NO_2$	3.7×10^{-12}	240	1
R8	$NO_2 + h\nu \rightarrow NO + O$			1
R9	$O + O_2 + M \rightarrow O_3 + M$	$k_0 = 5.6 \times 10^{-34}$	$(T/300)^{-2.8}$	1
R10	$HO_2 + O_3 \rightarrow OH + 2O_2$	1.1×10^{-14}	-500	2
R11	$OH + O_3 \rightarrow HO_2 + O_2$	1.6×10^{-12}	-940	2
R12	$NO + O_3 \rightarrow NO_2 + O_2$	2.0×10^{-12}	-1400	2
R13	$NO_2 + OH + M \rightarrow HNO_3 + M$	$k_0 = 2.6 \times 10^{-30}[N_2]$	$(T/300)^{-3.2}$	2
		$k_\infty = 2.4 \times 10^{-11}$	$(T/300)^{-1.3}$	2
R14	$NO_2 + O_3 \rightarrow NO_3 + O_2$	1.2×10^{-13}	-2450	1
R15	$NO_3 + NO_2 + M \rightarrow N_2O_5 + M$	$k_0 = 2.2 \times 10^{-30}[N_2]$	$(T/300)^{-3.9}$	2
		$k_\infty = 1.5 \times 10^{-12}$	$(T/300)^{-0.7}$	2
R16	$HO_2 + HO_2 \rightarrow H_2O_2 + O_2$	2.3×10^{-13}	600	2, 3
R17	$H_2O_2 + h\nu \rightarrow 2OH$			1
R18	$H_2O_2 + OH \rightarrow HO_2 + H_2O$	2.9×10^{-12}	-160	1
R19	$HO + HO_2 \rightarrow H_2O + O_2$	4.8×10^{-11}	250	2
R20	$HO + HO \rightarrow H_2O + O$	4.2×10^{-12}	-240	2
R21	$HO + HO + M \rightarrow H_2O_2 + M$	$k_0 = 6.9 \times 10^{-31}$	$(T/300)^{-0.8}$	2
		$k_\infty = 1.5 \times 10^{-11}$	-	2
R22	$CH_4 + OH \rightarrow CH_3 + H2O$	2.65×10^{-12}	-1800	2
R23	$CH_3 + O_2 + M \rightarrow CH_3O_2 + M$	$k_0 = 4.5 \times 10^{-31}$	$(T/300)^{-3.0}$	2
		$k_\infty = 1.8 \times 10^{-12}$	$(T/300)^{-1.7}$	2
R24	$CH_3O_2 + NO \rightarrow CH_3O + NO_2$	4.2×10^{-12}	180	1
R25	$CH_3O + O_2 \rightarrow CH_2O + HO_2$	3.9×10^{-14}	-900	2
R26	$CH_3O_2 + HO_2 \rightarrow CH_3O_2H + O_2$	3.8×10^{-13}	780	1
R27	$CH_3O_2H + h\nu \rightarrow CH_3O + OH$			1
R28	$CH_3O_2H + OH \rightarrow CH_3O_2 + H_2O$	1.9×10^{-12}	190	1
R29	$CH_2O + h\nu \rightarrow CHO + H$			1
R30	$CH_2O + OH \rightarrow CHO + H_2O$	1.0×10^{-11}	-	2
R31	$CHO + O_2 \rightarrow CO + HO_2$	3.5×10^{-12}	140	2
R32	$SO_2 + OH + M \rightarrow HOSO_2 + M$	$k_0 = 3.0 \times 10^{-31}$	$(T/300)^{-3.3}$	2
		$k_\infty = 1.5 \times 10^{-12}$	-	2
R33	$HOSO_2 + O_2 \rightarrow HO_2 + SO_3$	1.3×10^{-12}	-330	1
R34	$SO_3 + H_2O \rightarrow H_2SO_4$	2.4×10^{-15}	-	2
R35	$CFCl_3 + O(^1D) \rightarrow$ products			1, 10[a]
R36	$CFCl_3 + h\nu \rightarrow$ products			1, 10[a]
R37	$CF_2Cl_2 + O(^1D) \rightarrow$ products			1, 10[a]

Reaction [continued]		A, k_0, or k_∞	-E/R or f(T)	Ref.
R38	$CF_2Cl_2 + h\nu \rightarrow$ products			1, 10[a]
R39	$N_2O + h\nu \rightarrow N_2 + O(^1D)$			1, 10[a]
R40	$N_2O + O(^1D) \rightarrow 2NO$			1, 10[a]
R41	$N_2O + O(^1D) \rightarrow N_2 + O_2$			1, 10[a]
R42	$CF_3CH_2F + OH \rightarrow CF_3CHF + H_2O$	$1.7e^{-12}$	1750	2

References: 1) Atkinson *et al*., 1992; 2) DeMore *et al*., 1994; 3) Stockwell, 1995, 10) Wang *et al*., 1998

[a]: parameterized, current version of the model does not include predictions of stratospheric ozoen chemistry.

For bimolecular reactions, rate constants (cm^3/molecule/s) can be derived by

$$k(T) = A \exp\{(-E/R)(1/T)\}.$$

For termolecular reactions, rate constants (cm^3/molecule/s) can be derived by

$$k(T) = [k_0(T)[M]/(1 + k_0(T)[M]/k_\infty(T))]\ 0.6^a$$

Here, $a = 1/\{1 + [\log10(k_0(T)[M]/k_\infty(T))]^2\}$, $k_0(T) = k_0\ f(T)$, and $k_\infty(T) = k_\infty\ f(T)$.

Aqueous phase chemical reactions included in the global chemistry-climate model

Reaction		K_{298} (M or M atm^{-1})	-ΔH/R (K)	Ref.
R43	H_2SO_4 (g) ⇔ H_2SO_4 (aq)	infinite		
R44	H_2SO_4(aq) ⇔ HSO_4^- + H^+	1.00×10^3		4
R45	HNO_3 (g) ⇔ HNO_3 (aq)	$2.10 \times 10^5\ F_3$	8700	5
R46	HNO_3(aq) ⇔ NO_3^- + H^+	1.54×10^1	8700	5
R47	CH_2O(g) ⇔ $CH_2(OH)_2$	3.10×10^3	6500	6
R48	SO_2 (g) ⇔ SO_2 (aq)	$1.20\ F_4$	3100	7
R49	SO_2(aq) ⇔ HSO_3^- + H^+	1.23×10^{-2}	1960	7
R50	HSO_3^- ⇔ SO_3^{2-} + H^+	6.61×10^{-8}	1500	7
R51	H_2O_2(g) ⇔ H_2O_2 (aq)	$7.40 \times 10^4\ F_2$	6615	8
R52	OH(g) ⇔ OH(aq)	2.50×10^1	5280	9
R53	HO_2(g) ⇔ HO_2(aq)	$2.30 \times 10^3\ F_1$	6640	5
R54	HO_2(aq) ⇔ O_2^- + H^+	3.50×10^{-5}		4

References: 4) Perrin, 1982; 5) Schwartz, 1984; 6) Pandis and Seinfeld, 1989;
7) Smith and Martell, 1976; 8) Lind and Kok, 1986; 9) Jacob, 1986

The equilibrium constants are defined by:

$$K = K_{298} \cdot \exp\left\{\frac{-\Delta H}{R}\left(\frac{1}{T} - \frac{1}{298}\right)\right\}$$

Functions are defined as $F_1 = (1 + RE_8/[H^+])$, $F_2 = (1 + RE_{10}/[H^+])$, $F_3 = (1 + RE_{14}/[H^+])$, and $F_4 = (1 + RE_{16}/[H^+] + RE_{16} * RE_{17}/[H^+]^2)$.